GEOSPATIAL TECHNOLOGIES FOR CONSERVATION AGRICULTURE IN ARID ENVIRONMENT: A CASE STUDY OF URTACHIRCHIK DISTRICT, TASHKENT PROVINCE, UZBEKISTAN

By

Sarvar Khamidjonov

A THESIS

Submitted to
Michigan State University
in partial fulfillment of the requirements
for the degree of

Geography – Master of Science

2024

ABSTRACT

Conservation agriculture (CA) champions the sustainable use of land to elevate agricultural productivity and bolster environmental health. Central to CA practices, crop residues yield extensive benefits to both the ecosystem and farming systems by enhancing soil protection, conserving moisture, and facilitating nutrient cycling. The contributions highlight the necessity for spatial and temporal information to assess crop residue cover (CRC).

The daily availability of 3 m resolution observations from the PlanetScope constellation facilitates the mapping of small CRC areas, which remain undetectable at coarser spatial resolutions. Nonetheless, the application of the PlanetScope sensors for crop residue detection encounters challenges due to the absence of shortwave infrared (SWIR) bands. The bands are critical for identifying CRC in agricultural fields. To overcome the limitation, the study introduced a novel Normalized Difference Crop Residue Index (NDCRI), which innovatively employed visible, red-edge, and near-infrared (NIR) bands of PlanetScope imagery to quantify field-level CRC fractions, marking a pioneering use of the satellites in CRC assessment. Conducted in the study area, located within the Urtachirchik District of Tashkent Province, Uzbekistan, a country characterized by its arid environment —the research validated NDCRI's efficacy through comparison with field measurements, achieving goodness of fit (R^2) of 0.693 and root mean squared error (RMSE) of 19.15. The index's performance, verified through various regression analyses demonstrating its capability to estimate CRC, was also confirmed at different times across the research field and the district.

During data processing, the Normalized Difference Vegetation Index (NDVI) was used as a filtering criterion (NDVI < 0.22) to mitigate the impact of vegetation on the efficiency of the newly developed index.

Furthermore, in response to local conditions and needs, the research initiated an original concept to CRC policy, encompassing the strategic addition of crop residues from other fields to the study site.

ACKNOWLEDGEMENTS

I am deeply thankful for the chance to study at Michigan State University, a hub of growth, learning, and discovery. The university has equipped me with essential resources and knowledge for my research and motivated me to excel in my field.

I would like to express my deepest gratitude to all those who have made the completion of the thesis possible. First and foremost, I extend my sincere thanks to my supervisors Professor Jiaguo Qi and Professor Alim Pulatov for their invaluable guidance, patience, and expertise.

I am also immensely grateful to Professor David Roy, Professor Kyla Dahlin, and Professor Geoffrey Henebry whose expertise and knowledge were instrumental in shaping the direction and focus of the study.

I extend my heartfelt gratitude to the faculty, staff, peers, and colleagues at the Department of Geography, Environment, and Spatial Sciences, as well as the Center for Global Change & Earth Observations within the College of Social Science, for their unwavering support and the enriching discussions that have been instrumental in advancing my academic journey.

Furthermore, I must acknowledge the financial support received from the El-Yurt Umidi Foundation, which was pivotal in facilitating my study activities.

I also extend profound gratitude to my home institution, the “Tashkent Institute of Irrigation and Agricultural Mechanization Engineers” National Research University, as well as to the researchers from the EcoGIS Center who offered their insights and time, both of which were crucial to the success of the research.

On a personal note, I wish to express my heartfelt appreciation to my family and friends for their steadfast support, understanding, and love throughout the challenging yet rewarding endeavor.

Completing the thesis has been a significant journey, and the encouragement and support of each one mentioned have been invaluable.

Thank you!!!

TABLE OF CONTENTS

LIST OF ABBREVIATIONS

AI – Artificial Intelligence

CA – Conservation Agriculture

CRC - Crop Residue Cover

CTIC - Conservation Technology Information Center

ESRI - Environmental Systems Research Institute

FAO - Food and Agriculture Organization

GPS - Global Positioning System

IPCC - Intergovernmental Panel on Climate Change

NASA - National Aeronautics and Space Administration

NDCRI - Normalized Difference Crop Residue Index

NDVI - Normalized Difference Vegetation Index

NIR – Near-Infrared

OLS - Ordinary Least Squares

RMSE - Root Mean Squared Error

SWIR - Shortwave Infrared

TA - Traditional Agriculture

USDA - United States Department of Agriculture

UN - United Nations

SDGs - Sustainable Development Goals

CHAPTER 1: INTRODUCTION

1.1 Fundamentals of Conservation Agriculture

Agriculture in the 21st century confronts a myriad of diverse and complex challenges, ranging from urban sprawl to the necessity of sustainable nutrient management, all demanding immediate and innovative responses (Sims et al., 2013; Blinn et al., 2022). With the global population expected to surge to 10 billion by 2050 (The World Bank, 2024), there is an escalating demand for a substantial increase in food production (Van Dijk et al., 2021). Concurrently, the global community is facing the critical urgency to protect Earth's limited resources, highlighting the need for sustainable solutions (Hoekstra & Wiedmann, 2014). In addressing the multifaceted agricultural challenges, conservation agriculture (CA) emerges as a strategic approach, advocating for sustainable land management practices that not only safeguard the environment but also support climate change adaptation and mitigation (IPCC Climate Change, 2022; FAO, 2024). By focusing on practices that conserve, enhance, and make efficient use of natural resources through the integrated administration of soil, water, and biological resources, CA offers a sustainable alternative to traditional agricultural (TA) methods, which often overlook the importance of resource conservation and sustainable management (Somasundaram et al., 2020). Therefore, the drive towards sustainable agricultural operations becomes crucial, aiming to maintain or improve current productivity levels without further environmental degradation, thereby addressing global concerns related to food security and the preservation of ecological integrity (Zheng et al., 2014). According to the Food and Agriculture Organization (FAO) (2024), CA operates on three core principles that are tailored to meet the specific conditions and requirements of local areas. The principles include minimal mechanical disturbance of the soil, maintaining a permanent organic cover on the soil, and promoting species diversification.

FAO (2024) also highlights several significant advantages of CA across economic, agronomic, and environmental domains. Economically, CA provides substantial benefits by saving time and reducing labor requirements, which in turn lowers costs associated with fuel, machinery operation, and maintenance. Additionally, the approach leads to higher efficiency by generating more output from fewer inputs. Agronomically, CA enhances the amount of organic matter in the soil, conserves water within the soil, and improves the soil structure, which benefits the rooting zone of plants. From an environmental perspective, CA contributes to reducing soil erosion, which can decrease maintenance costs for roads, dams, and hydroelectric power plants. It also aids in

improving water and air quality, increases biodiversity, and enhances carbon sequestration. Furthermore, CA practices directly contribute to several of the United Nations (UN) Sustainable Development Goals (SDGs) (2015) designed for 2030. By augmenting agricultural productivity and resilience, CA helps to ensure food security for an expanding global population, thereby supporting the SDG of zero hunger (Goal 2). In terms of climate action (Goal 13), CA techniques such as reduced tillage and cover cropping contribute to carbon sequestration in the soil, which aids in mitigating the impacts of climate change. Finally, CA encourages soil health and terrestrial ecosystems by minimizing soil erosion and enhancing biodiversity, aligning with the SDG of life on land (Goal 15).

1.2 Conservation Agriculture in Uzbekistan

Uzbekistan's agricultural sector plays a vital role in the nation's economy, accounting for 28% of gross domestic product (GDP) and employing a significant portion (around 25%) of the workforce (FAO, 2023). However, the crucial industry faces challenges due to dwindling water resources and declining soil fertility (FAO, 2023). Recognizing the threats, the Decree on the Strategy for the Development of Agriculture in the Republic of Uzbekistan for 2020-2030, issued by the President, prioritizes the sustainable management of land and water resources alongside increased food production and environmental protection (LexUZ, 2019). In such a context, CA presents itself as a promising solution, offering benefits like enhanced soil health, reduced erosion, and improved water retention, thus contributing to a more sustainable agricultural future for Uzbekistan.

Studies in Uzbekistan's irrigated agricultural lands demonstrate the effectiveness of CA practices. Research shows that CA techniques such as reduced tillage and residue retention can improve soil health in several ways. They link to decreased soil salinity, increased soil moisture retention (Egamberdiev, 2007; Pulatov et al., 2012; Devkota et al., 2015), and reduced soil erosion and compaction (Pulatov, 2007; Khaitov & Allanov, 2014). Beyond the soil benefits, CA offers the potential to maintain crop yields while requiring less time, energy, and resources compared to conventional tillage practice (FAO, 2009; Pender et al., 2009; Devkota et al., 2013).

1.3 The Role of Crop Residue in Conservation Agriculture

Crop residue cover (CRC) is the primary physical variable that directly indicates the application of CA practices (Wang et al., 2023). Crop residue, encompassing standing dead vegetation, surface

plant litter, and residues left after crop harvest, such as corn stalks or soybean stubble, refers to non-photosynthetic vegetation that accumulates on the soil surface of farmlands following harvest completion and crop senescence (Hively et al., 2018; Pepe et al., 2020; Wang et al., 2023). The percentage of CRC on the soil surface is frequently utilized as an indicator of tillage intensity (Hively et al., 2018). Tillage methods are then categorized based on the levels of CRC observed post-planting, such as traditional tillage for less than 15% cover, low residue tillage for 15–30% cover, conservation tillage for 30–60% cover, and high residue tillage for more than 60% cover (CTIC, 2022). Lower coverage classes are linked to increased erosion risks from rain and wind, with more than 30% residue cover typically preventing about 65% of erosion—varying by soil type, slope, and local conditions—while coverage above 60% can inhibit over 90% of erosion (Papendick et al., 1990; Godwin, 1990; Hively et al., 2018).

Managing crops with high residue levels is key to sustainable systems, working alongside reduced chemicals, better nutrient management, and varied crop rotations (Hobbs et al., 2008; Delgado, 2010). When integrated with other CA practices like minimal tillage and crop rotation, retaining crop residue helps minimize negative environmental impacts and enhances the soil's structural components and processes within the agroecosystem (Ranaivoson et al., 2017). Moreover, effective crop residue administration goes beyond just crop production; it plays a crucial role in advancing environmental sustainability by facilitating the evaluation of agricultural practices and contributing to the development of sustainable management plans and policies (Zheng et al., 2014).

1.4 Evaluating Crop Residue Cover from the Ground Up: A Review

The fraction of soil covered by crop residues is determined after the harvest of the previous crop, subsequent tillage, and the planting of the next crop (CTIC, 2022). The measurements, particularly for crops that contribute significantly to crop residues like wheat, corn, and soybeans, are conducted during the summer months in both the Southern and Northern Hemispheres (USDA, 2024). The window for measuring CRC is narrow, closing once new crop growth obscures the soil surface (Hively et al., 2018). The amount of residue cover on agricultural fields is mostly assessed using three ground-based methods: line-transect, roadside surveys, and in-field photography.

In the line-transect method, a long cord marked with evenly spaced intervals is stretched diagonally across a field, and observers visually count the instances where the markers touch pieces of crop residue on the ground, providing data for estimating the overall percentage of CRC (Morrison et

al., 1993).

Roadside surveys for identifying CRC traditionally relied on visual inspection of adjacent fields. To address limitations in efficiency and accuracy, Pilger et al. (2020) have developed vehicle-mounted camera systems specifically suited for the task.

The photographic method for CRC assessment involves capturing single or multiple top-down view photographs of the field (Yue et al., 2019), followed by image segmentation analysis to estimate the percentage of soil surface obscured by residue in the images (Wang et al., 2023).

1.5 Advances in Crop Residue Detection Using Remote Sensing Techniques: A Review

Remote sensing technology enables the monitoring of CRC across vast agricultural areas simultaneously without the need for physical presence in each field, thereby facilitating large-scale analysis with reduced labor and resources.

The pioneering efforts in the domain can be traced back to the mid-1970s to 1980s, initiated by Gausman et al. (1975). Subsequently, numerous scientific investigations have been conducted to refine the remote sensing techniques and indices (Table 1) for the accurate evaluation of crop residue. Some important advancements include the development of the Normalized Difference Tillage Index (NDTI) by Van Deventer et al. (1997) for multispectral medium spatial resolution Landsat TM and ETM+, the Cellulose Absorption Index (CAI) by Daughtry et al. (2005, 2006) for hyperspectral medium spatial resolution AVIRIS and Hyperion, and the Lignin Cellulose Absorption Index (LCA) and the Shortwave Infrared Normalized Difference Residue Index (SINDRI) by Daughtry et al. (2005) and Serbin et al. (2009a), correspondingly, for another multispectral medium spatial resolution sensor (ASTER). Additionally, Bannari et al. (2006) and Hively et al. (2018) have explored CRC measurement using high-resolution multispectral satellite imagery from IKONOS and WorldView-3, respectively. Finally, Watts et al. (2011) and Zhou et al. (2021) have developed models specifically for the MODIS and Sentinel-2 satellite sensors, accordingly, to quantify CRC. All the contributions have significantly advanced the field of remote sensing for crop residue monitoring.

Despite the use of varied tillage indices across different sensors on various platforms, the underlying principle for the indices is rooted in the absorption characteristics of cellulose and lignin between the 2100 and 2300 nm wavelength (Figure 1), where residues display unique absorption features compared to soils in the shortwave infrared (SWIR) region, distinct from the

visible and near-infrared (NIR) regions (Asner & Lobell, 2000; Daughtry, 2001; Daughtry et al., 2004).

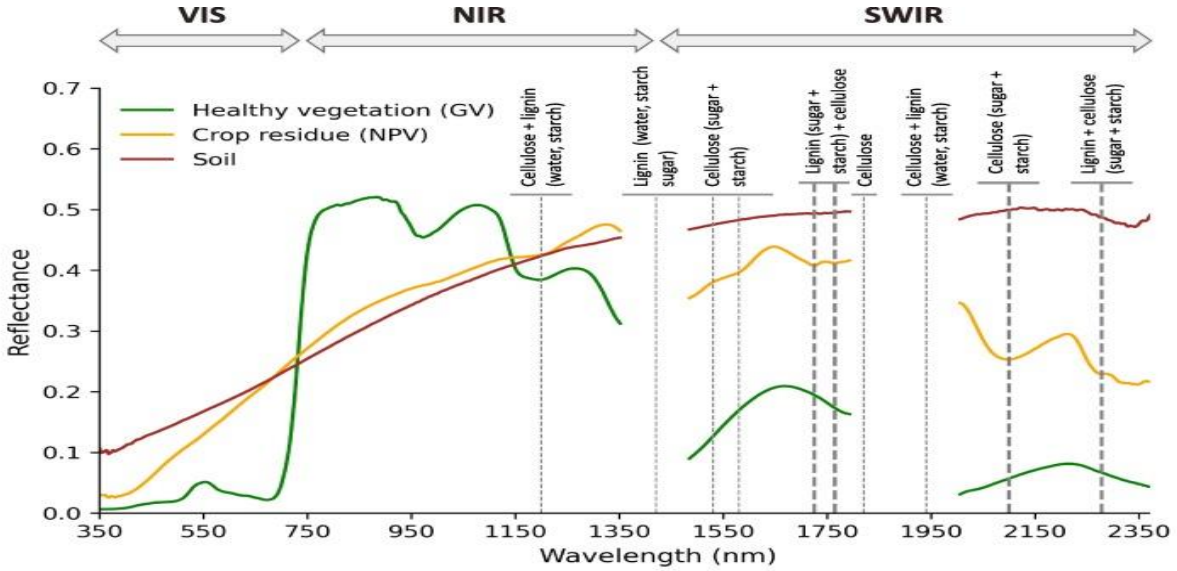

Figure 1. Shown are three exemplary spectra (healthy green crop, soil, and crop residue) (Verrelst et al., 2023) from maize and wheat fields of the Munich-North-Isar in Germany (Wocher et al., 2018).

Table 1. Satellite-based crop residue indices.

Satellite	Crop Residue Index	Abbreviation	Formula	Reference
Landsat	Normalized Difference Index 7	NDI7	(NIR-SWIR2)/(NIR+SWIR2)	Mcnairn & Protz (1993)
	Normalized Difference Tillage Index	NDTI	(SWIR1-SWIR2)/(SWIR1+SWIR2)	Van Deventer et al. (1997)
	Simple tillage index	STI	SWIR1/SWIR2	Van Deventer et al. (1997)
	Normalized Difference Residue Index	NDRI	(Red-SWIR2)/(Red+SWIR2)	Gelder et al. (2009)
ASTER	Lignin Cellulose Absorption	LCA	100(2x SWIR6−SWIR5−SWIR8)	Daughtry et al. (2005)
	Shortwave Infrared Normalized Difference Residue Index	SINDRI	(SWIR6-SWIR7)/(SWIR6+SWIR7)	Serbin et al. (2009a)
Hyperion	Cellulose Absorption Index	CAI	0.5x(Reflectance at 2000 nm+Reflectance at 2200 nm)-Reflectance at 2100 nm	Daughtry et al. (2006)
MODIS	Dead Fuel Index	DFI	100x(1-Reflectance at Band7/Reflectance at Band6)x(Reflectance at Band1/Reflectance at Band2)	Cao et al. (2010)

Table 1. (cont'd).

Sentinel-2	Simulated Cellulose Absorption Index	3B1	100x(0.5x(Blue+SWIR2)-Red)	Ding et al. (2020)
	Simulated Lignin Cellulose Absorption Index	3B2	(Blue-Red)/(Blue+SWIR2)	Ding et al. (2020)
	Simulated NDRI	3B3	(SWIR2-Red)/(SWIR2+SWIR1)	Ding et al. (2020)

1.6 Problem Statement

Previous studies about CA in Uzbekistan have mostly focused on the adoption of CA in the area and its benefits to the local environment. However, research on estimating CRC, one of the fundamental aspects of CA, using ground-based methods or remote sensing techniques is almost non-existent.

Although established ground-based methods like line-transect, roadside surveys, and photography accurately monitor CRC for specific locations, their application across vast areas becomes time-consuming and expensive due to the need for on-site surveys. Thus, traditional field methods struggle to offer prompt insights into the intensity of tillage across extensive areas for every field (Zheng et al., 2014) and are primarily useful for calibrating data for remote sensing techniques.

In assessing CRC, whereas remote sensing may not match the accuracy of field measurements, it offers significant savings in time and costs. Prior research has explored crop residue quantification or tillage intensity employing sensors mounted on both airborne and satellites.

Airborne data offers valuable insights for agricultural management and conservation practices. High-resolution imagery captured from airborne platforms allows for the detection of CRC across agricultural fields. Airborne hyperspectral remote sensing, with its ability to capture a wide range of wavelengths across the optical spectrum (400-2400 nm), demonstrates high accuracy (>90%) in identifying CRC (Daughtry et al., 2005) compared to the multispectral sensor, which is unsuccessful in executing the task (Kosmowski et al., 2017). It highlights the advantage of hyperspectral data's rich and narrowband information for accurate residue cover detection. Nevertheless, it is important to acknowledge the limitations associated with airborne hyperspectral data for the application. The limitations include the restricted area covered during a single flight, potential disruptions caused by cloud cover, and the need for strategic planning to ensure suitable weather conditions for data collection over the desired research areas.

Despite hyperspectral (Hyperion) and multispectral (Landsat, Sentinel-1) satellite remote sensing data, with an accuracy of approximately 75-80% (Daughtry et al., 2006; Azzari et al., 2019) for measuring CRC, do not match the results of airborne hyperspectral data, they still serve as effective tools for acquiring consistent and unbiased crop residue data across large expanses (Zheng et al., 2012). Nonetheless, while the limitations of airborne data tend to be general, the limitations of each satellite remote sensing system are specific. Hyperion (no longer operational) suffers from low temporal coverage due to its sensor being activated only upon request (Zheng et al., 2012).

ASTER's SWIR detector malfunctioned in April 2008 (Serbin et al., 2009b). IKONOS (no longer operational) and WorldView-3, yet offering high spatial resolution, have limited coverage areas and come at a significant cost. MODIS data, albeit providing global daily coverage, suffers from coarse spatial resolution. National Aeronautics and Space Administration (NASA) Harmonized Landsat Sentinel-2 (HLS, Claverie et al., 2018) provides high temporal frequency data by combining Landsat and Sentinel-2, but the 30 m multispectral satellite data may have uncertainties when compared with point measurements of CRC in fields (Wang et al., 2023).

The analyzed scientific studies predominantly have focused on SWIR wavelengths of 2000–2200 nm, which, among all spectral wavelengths, contribute most significantly to the quantification of CRC (Nagler et al., 2003). However, while NIR wavelengths in the range of 900–1100 nm, as well as red and red-edge wavelengths in the range of 600–750 nm, also demonstrate high predictive capabilities for CRC (Yue et al., 2020; Wang et al., 2023), investigations using only the bands themselves—without the inclusion of SWIR bands—are not observed in satellite imagery studies so far.

Green vegetation not only physically conceals crop residue but also interferes with the measurement of crop residue in satellite images due to high water content (Zheng et al., 2014). Daughtry et al. (2005) recommended excluding pixels containing green vegetation using vegetation indices; predominantly, the Normalized Difference Vegetation Index (NDVI) (Rouse et al., 1974) less than 0.3 was utilized (Daughtry et al., 2004; Serbin et al., 2009a; Hively et al., 2018) to restrict analysis to areas without significant green vegetation, although the maturity periods of crops, which can also have an NDVI value of less than 0.3, were largely overlooked.

To address the challenges identified in existing studies, we aimed to develop a new index by using the bands of the PlanetScope sensors to estimate CRC. The PlanetScope constellation, which began launching in November 2018 and comprises approximately 200 satellites, is capable of imaging the entire land surface of the Earth daily, equating to a collection capacity of 350 million km² per day (Planet Team, 2023). The study demonstrates, for the first time, the potential of 3 m resolution PlanetScope imagery for crop residue mapping in the context of Uzbekistan. The PlanetScope constellation's high spatial and temporal resolution observations, along with its extensive global coverage, could facilitate the mapping of small CRC areas that go undetected by coarse spatial resolution techniques. Nevertheless, there are two main challenges: (i) due to PlanetScope being a commercial satellite, the imagery it provides is costly, and (ii) the sensors capture imagery in

visible, red-edge, and NIR spectra, but not in SWIR spectrum, which is crucial for CRC mapping (Asner & Lobell, 2000; Daughtry, 2001; Daughtry et al., 2004). The first issue is resolved by allowing researchers to freely download data from PlanetScope by Planet company (which is uncommon among other commercial satellite companies), albeit with a monthly cap on spatial coverage (5000 km²/month) designated for scientific research. A solution for the second problem is found through the importance of spectral bands in detecting CRC, as identified by Yue et al., (2020) and Wang et al., (2023). Namely, it is shown that wavelengths in NIR, red-edge, and red, besides SWIR wavelengths, can also predict CRC, providing us with the possibility to monitor CRC from satellite images without the need for SWIR bands. Sullivan et al. (2006), despite through a hand-held thermal infrared imager, managed to quantify CRC with high accuracy by employing NIR and blue bands, which adds an extra incentive to our research.

Furthermore, to mitigate the impact of vegetation on the newly developed index for assessing CRC, NDVI is utilized as a filtering criterion, taking into consideration the crop maturity period.

Significantly, the reviewed studies have been conducted in locations characterized by humid environments, including Ohio (Van Deventer et al., 1997; Azzari et al., 2019), Maryland (Daughtry et al., 2005; Serbin et al., 2009a; Hively et al., 2018), Iowa (Daughtry et al., 2006; Gelder et al., 2009); Azzari et al., 2019), Montana (Watts et al., 2011), Indiana (Zheng et al., 2012; Azzari et al., 2019), Illinois (Azzari et al., 2019; Wang et al., 2023), Ontario (Mcnairn & Protz, 1993), Saskatchewan (Bannari et al., 2006), Northern India (Zhou et al., 2021), and Northeast China (Ding et al., 2020; Gao et al., 2022) (Figure 2). In contrast, our research focuses on a study area in Uzbekistan, which features an arid environment (Figure 2). Factors such as soil water content, mineral composition, and the presence of contaminants may influence the spectral reflectance of soil in arid settings, resulting in distinct spectral characteristics compared to soils in humid environments (Ben-Dor et al., 2008; Philpot, 2014; Fabre et al., 2015). Consequently, the difference previously noted in the spectral reflectances of soil and crop residue (Figure 1) may extend beyond SWIR bands to include other bands as well.

It is important to note that the effectiveness of CRC practice depends on local conditions and requirements. Existing CRC strategies may not fully correspond to the specificities, thereby underscoring the necessity for innovative approaches. There is always an opportunity to investigate novel modifications to CRC policies, aiming to improve agriculture practices tailored to particular environmental settings.

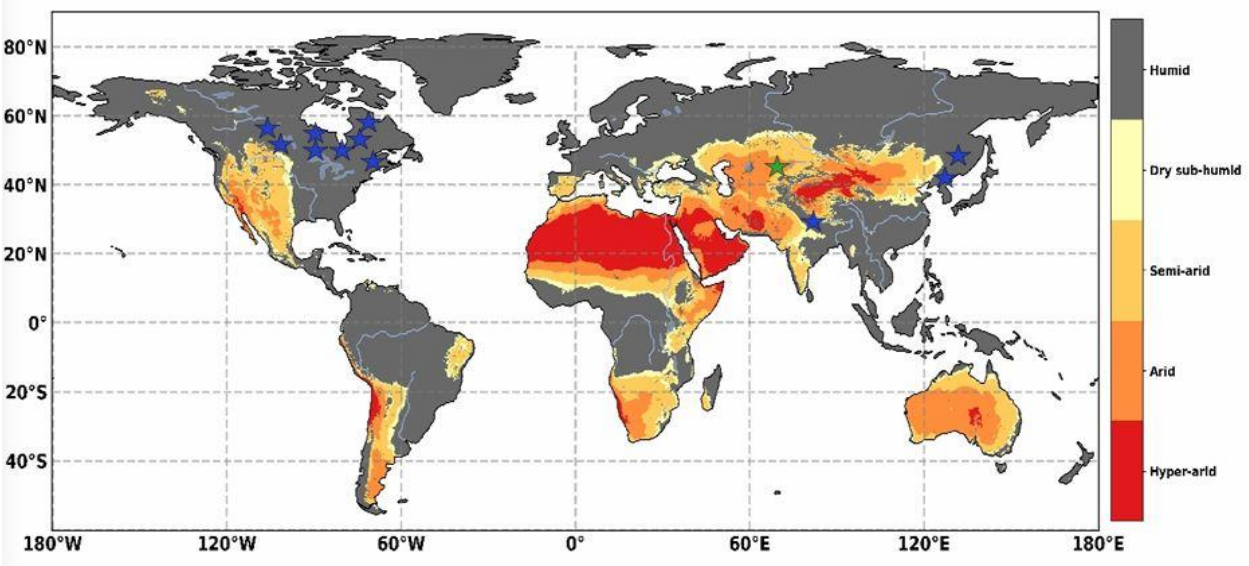

Figure 2. Geographical distribution of drylands, delimited based on the aridity index (AI). The classification of AI is: Humid AI > 0.65, Dry sub-humid 0.50 < AI ⩽ 0.65, Semi-arid 0.20 < AI ⩽ 0.50, Arid 0.05 < AI ⩽ 0.20, Hyper-arid AI < 0.05 (Abatzoglou et al., 2018), (blue stars – locations of the reviewed studies, green star – location of our research area).

1.7 Research Objectives

The objectives of the study are (i) to demonstrate the utility of high-resolution PlanetScope imagery by evaluating the predictive capabilities of NIR, red-edge, and red wavelengths for monitoring CRC, (ii) to develop and validate the novel spectral index for CRC quantification, (iii) to analyze the accuracy and efficiency of CRC detection in arid environment, (iv) to investigate a new NDVI threshold as a filter in identifying CRC, taking into account the crop maturity period, and (v) to explore the potential of integrating an original concept into CRC policy to address specific local challenges.

CHAPTER 2: RESEARCH LOCALE AND DATA SOURCES

2.1 Study Area Location

Uzbekistan is a doubly landlocked country which is located in Central Asia between the Syr Darya and the Amu Darya rivers (Figure 3). The total territory of the republic is 447,400 km^2, of which just less than 43,000 km^2 is used for agricultural purposes. Unique climate conditions, consisting of immensely cold winters, wet and cool falls, and dry, long, and extreme summers, could only be observed in Uzbekistan (FAO, 2011).

Tashkent Province, with its capital Nurafshon, is situated in the North-Eastern part of the country, nestled between the Syr Darya River and the Tien Shan Mountains, and shares its borders with Kyrgyzstan, Tajikistan, the Sirdaryo Region, and the Namangan Region (Figure 4). The province spans an area of 15,600 km^2, with over 20% dedicated to agriculture (UZSTAT, 2023). The water supply for the province primarily originates from the Chirchik and Akhangaran river basins.

Urtachirchik is located in the middle of Tashkent Province (Figure 4). The climate in the district is arid continental. The absolute summer mean maximum temperature is +36°C (Mirshadiev, 2015). The area of Urtachirchik District is 510 km^2. The vegetation period is about 200 days (Gerts et al., 2020).

The study area itself is situated within the fields of the Research Education Center at the "Tashkent Institute of Irrigation and Agricultural Mechanization Engineers" National Research University, located in the Urtachirchik District of Tashkent Province, Uzbekistan, covering 0.05 km^2 with dimensions of 500 m in length and 100 m in width (Figure 4). The fields are positioned on the right bank of the Karasu River, a tributary of the Akhangaran River. The starting point of the experimental field is positioned at coordinates 41°02'16"N latitude and 69°01'15"E longitude, at an altitude of 355 meters.

The primary crops in Uzbekistan are winter wheat (*Triticum aestivum*), typically sown from September to November and harvested from May to July, and cotton (*Gossypium hirsutum*), which is planted from April to May and harvested from September to November. Following the harvest of the main crops, lands in Uzbekistan are often used for secondary cropping, involving the cultivation of vegetables (various species), legumes (e.g., *Phaseolus vulgaris*), potatoes (*Solanum tuberosum*), and corn (*Zea mays*).

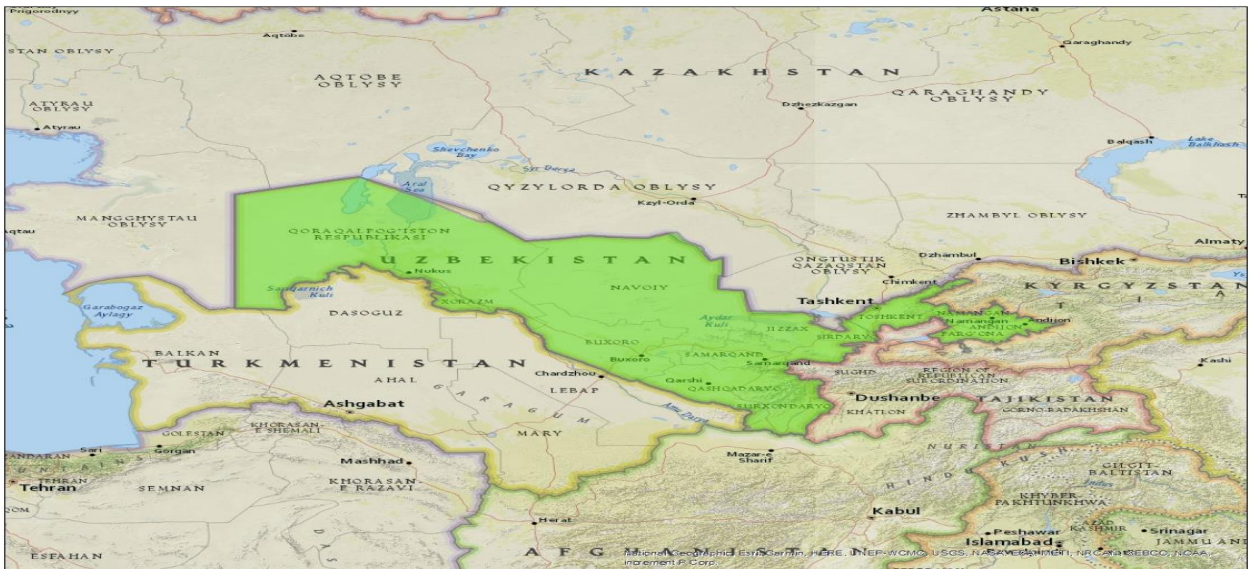

Figure 3. Map of Central Asia, highlighting Uzbekistan.

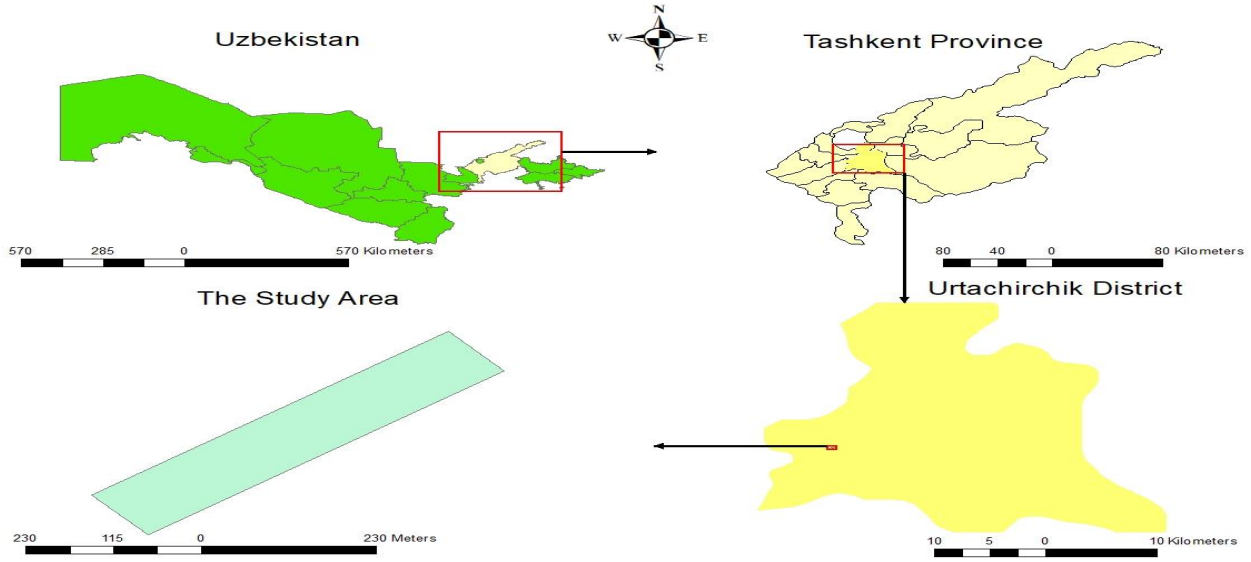

Figure 4. Nested maps illustrating the geographic context of the study area within the Urtachirchik District, Tashkent Province, Uzbekistan.

In alignment with national agricultural practices, winter wheat was planted in the study area in December 2021 (Table 2) using traditional methods, which include tillage. In February 2022, to evaluate the impact on the current winter wheat yield and as an augmentative measure for the CA practice commencing after the crop cycle, rice residue from another field was transported to our research site and applied to cover more than 50% of the land. Subsequently, the winter wheat harvest was completed by July 2022, and in August 2022, one month later, the field was replanted with mung bean (*Vigna radiata*), demonstrating a rapid shift to secondary cropping. Figure 5

displays a collection of photographs from the field, illustrating different stages of the crop cycle over the observed period.

Figure 5. Pictures from the research area: (A) winter wheat after planting (January), (B) covering process of winter wheat using residue transported from another field (February) (C) winter wheat in the greening phase (May), (D) winter wheat in the mature stage (June), (E) winter wheat post-harvest (July), (F) preparation for sowing the next crop (mung bean) (August).

Table 2. Timeline of agricultural activities for crop monitoring in the study area (Pulatov, in press).

Time Period	Agricultural Activity
Early December 2021	Planting of winter wheat
Late February 2022	Winter wheat covered with rice residue from another field
Late April-Early May 2022	Winter wheat in the green-up phase
Mid-June 2022	Winter wheat reaching maturity
Early July 2022	Harvesting of winter wheat
Early August 2022	Planting of mung bean

2.2 Field Data Acquisition

After the winter wheat harvest, the study area was artificially segmented into 72 sub-fields, each measuring 55 m long and 12.5 m wide. Afterwards, winter wheat residue from specific sub-fields was manually cleared and relocated to other sub-fields, which already contained a quantity of old (i.e., transferred from another field earlier in the year) and undecomposed rice residue. Consequently, two distinct groups emerged: one consisting of 40 sub-fields almost completely covered with winter wheat residue and rice residue (in small quantities) and another comprising 32 sub-fields with minimal or no residue, prepared for CA and TA practices, respectively (Figure 6). Mung bean was then sown in the residue-rich sub-fields using CA techniques (i.e., no-tillage), whereas TA methods (i.e., with tillage) were applied to the sub-fields lacking residue.

On 10 August 2022, two days after planting the mung bean in the study area, on-site measurements were taken from 20 sample locations (Figure 7), with management practices ranging from tillage to no-till. According to the Kaunchi meteorological station, situated in Tashkent Province at latitude 41°05' N, longitude 69°00' E, at an elevation of 344 m and approximately 8 km from the research site (Figure 8), there was no rainfall recorded in the month leading up to the sampling (Figure 9). Additionally, the maximum and minimum air temperatures on the sampling day were 33.4°C and 22.7°C, respectively (Figure 10).

Conservation Agriculture sub-fields Traditional Agriculture sub-fields

72	64	56	48	40	32	24	16	8
71	63	55	47	39	31	23	15	7
70	62	54	46	38	30	22	14	6
69	61	53	45	37	29	21	13	5
68	60	52	44	36	28	20	12	4
67	59	51	43	35	27	19	11	3
66	58	50	42	34	26	18	10	2
65	57	49	41	33	25	17	9	1

Figure 6. Layout of the study area divided into 72 sub-fields (Note: Numbering of the sub-fields begins from the lower right corner, corresponding to the starting point of the field).

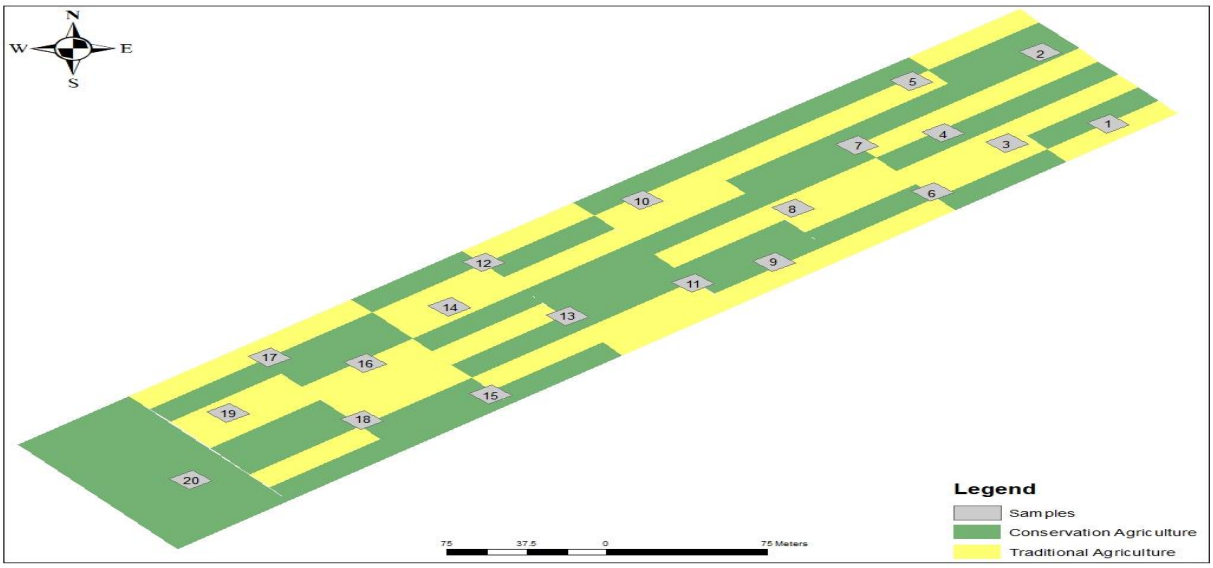

Figure 7. Map of the research field showing 20 sample locations with conservation and traditional sub-fields (Note: Numbering of the sample locations begins corresponding to the starting point of the field).

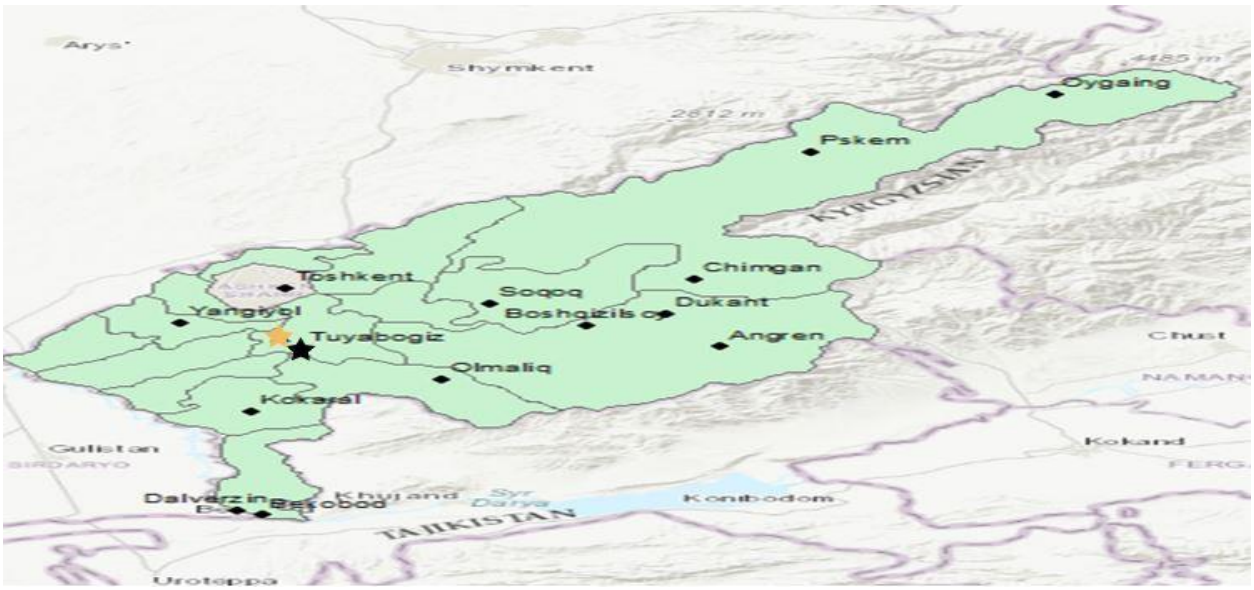

Figure 8. Locations of the study area (gold star), the Kaunchi meteorological station (black star), and other meteorological stations (black points) in Tashkent Province.

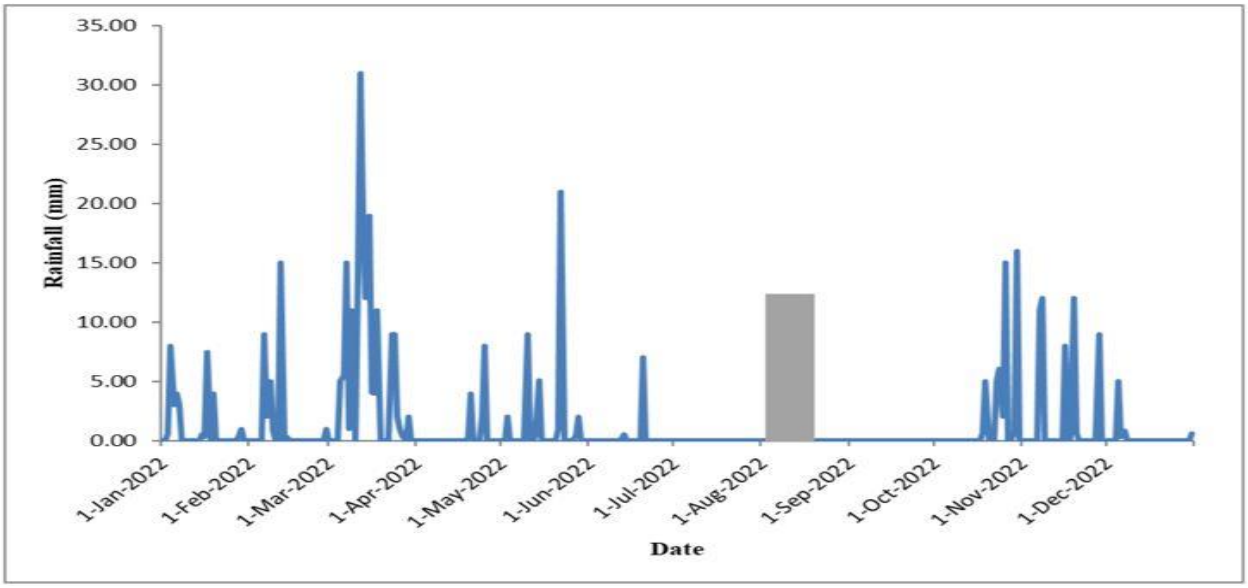

Figure 9. Precipitation change in the study area during 2022 (Note: The sampling day (August 10) is highlighted in the graph).

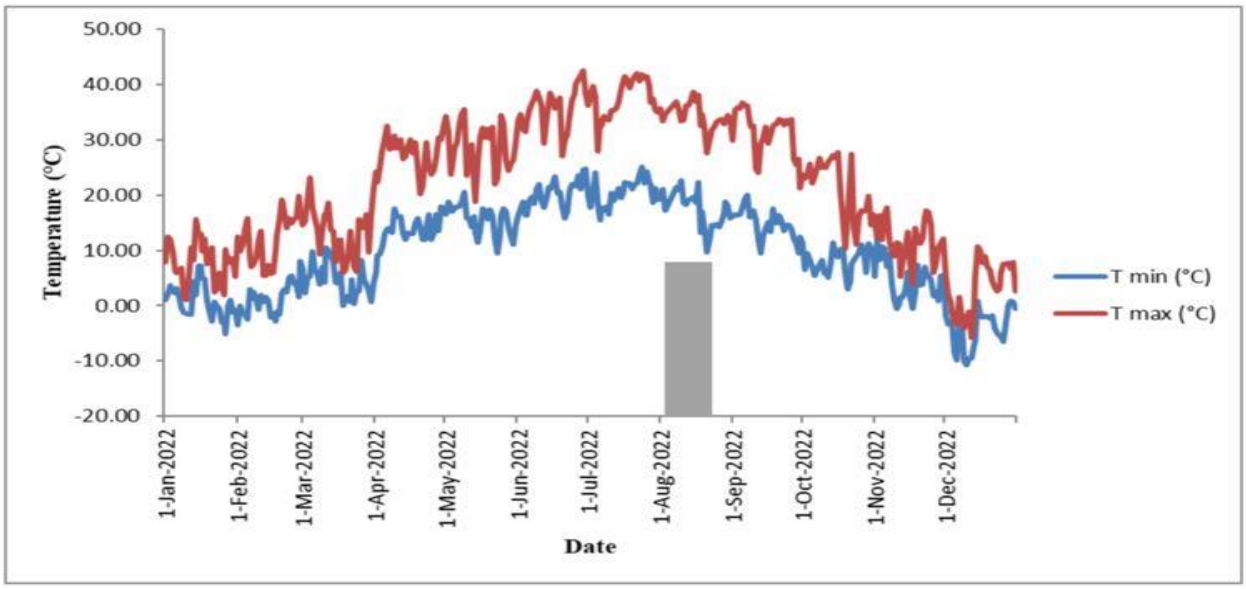

Figure 10. Temperature change in the study area during 2022 (Note: The sampling day (August 10) is highlighted in the graph).

2.3 Remote Sensing Imagery Collection

When the research commenced, product supply from the first two sensor generations of PlanetScope, Dove-Classic and Dove-R, had almost ceased (April 2022) (Planet Team, 2023). Consequently, images from the third generation (SuperDove) were utilized. The study employed atmospherically corrected, 3 m orthorectified 16-bit products (Level 3B), each covering approximately 32.5 km × 19.6 km. For further insights, Table 3 outlines the reflectance band wavelength ranges specific to PlanetScope imagery (Planet Team, 2023) and their interoperability with Sentinel-2 (Planet Developers, 2024).

For comparison with field measurements and calibration of the new index, a single scene product (as the field is a small size) that covers the study area, captured on August 10, 2022—the day when the field measurements were conducted—was utilized as the main image. Subsequently, five images of the research field captured at various stages of the crop cycle (see Table 2), spanning from March to August (August 4, 2022; July 7, 2022; June 18, 2022; May 12, 2022; and March 2, 2022) and each consisting of a single scene, were employed to verify the results through temporal analysis. In addition, five images of the entire Urtachirchik District, from May to August (August 6, 2022; July 8, 2022; June 18, 2022; June 2, 2022; and May 12, 2022), corresponding closely to the dates of the study area images and each comprising three to eight scenes (as the district is a

relatively large size), were used to test the obtained findings. The images of the district were then mosaicked using ArcGIS Desktop 10.8.2 (ESRI, 2022). Importantly, the PlanetScope 3 m Usable Data Mask (UDM2), categorizing each pixel based on its condition—clear, cloud, cloud shadow, haze, snow, missing, or flagged as suspect due to saturation or downlink errors (Planet Team, 2023)—was included as a supplementary layer with the primary images during download.

Table 3. Reflectance band wavelength ranges for PlanetScope imagery (Planet Team, 2023) and their interoperability with Sentinel-2 (Planet Developers, 2024).

Band	Name	Range (nm)	Interoperable with Sentinel-2
1	Coastal Blue	431-452	Yes - with Sentinel-2 Band 1
2	Blue	465-515	Yes - with Sentinel-2 Band 2
3	Green I	513-549	No equivalent with Sentinel-2
4	Green	547-583	Yes - with Sentinel-2 Band 3
5	Yellow	600-620	No equivalent with Sentinel-2
6	Red	650-680	Yes - with Sentinel-2 Band 4
7	Red Edge	697-713	Yes - with Sentinel-2 Band 5
8	Near-infrared	845-885	Yes - with Sentinel-2 Band 8a

CHAPTER 3: METHODS

3.1 Field Measurement Strategies: The Line-Transect Approach

For each sampling location, CRC was quantified employing the line-transect method as described by Morrison et al., (1993). A 15-meter tape marked at 0.3-meter intervals, dividing it into 50 sections, was utilized for measurements. At every sampling site, the tape was laid diagonally across the rows (Bonham, 1989), and intersections of crop residue with the marked sections were tallied. The process was repeated on an adjacent diagonal, and the percentage of CRC was determined by averaging the two intersection counts. The central location of the pair of line-transects was recorded using a Garmin global positioning system (GPS) 72 device (Figure 11) with a positional accuracy of 5.2 meters.

Figure 11. Use of Garmin GPS 72 device in the field for location measurements.

3.2 Satellite Imagery Analysis for Crop Residue and Vegetation Indexing

SWIR bands are notably the most significant contributors to CRC quantification among all spectral bands (Nagler et al., 2003). Additionally, Sentinel-2 satellite observations reveal that NIR, red, and red-edge bands, following SWIR bands, similarly demonstrate substantial predictive capabilities for CRC (Figure 12) (Yue et al., 2020; Wang et al., 2023). Although the PlanetScope constellation lacks SWIR bands, the image taken on August 10, 2022, for the research area corroborated the findings of the aforementioned studies. When areas with already known CRC (n=5) and without CRC (n=5) were delineated with special polygons in the image (Figure 13), alongside the previously mentioned bands (NIR, red, and red-edge), also yellow band, not present in Sentinel-2, recorded higher results than other bands (coastal blue, blue, green, and green_i) for CRC assessment in the spectral profile (Figure 14) created using ArcGIS Pro 3.0.0 software (ESRI, 2022). Furthermore, significant differences (>0.05 in reflectance values) were noted between areas with and without CRC, spanning from yellow to NIR bands. On the contrary, from coastal blue to green bands, differences observed between areas with and without CRC ranged from zero to minimal (<0.035 in reflectance values).

Building on similar findings, Sullivan et al. (2006) created the Crop Residue Cover Index (CRCI) by using NIR (which shows a substantial difference between areas with and without CRC) and blue (which shows a minimal difference between areas with and without CRC) bands, as a normalized ratio from a hand-held thermal infrared imager, achieving approximately 85% accuracy in monitoring CRC. Moreover, the well-known Normalized Difference Vegetation Index (NDVI) (Rouse et al., 1974) utilizes the significantly higher reflectance of vegetation in NIR band (analogous to the performance of yellow, red, red-edge, and NIR bands in CRC assessment as shown in Figure 14) compared to its considerably lower reflectance in red band (akin to the performance of coastal blue, blue, green_i, and green bands in CRC detection in Figure 14) to identify healthy vegetation.

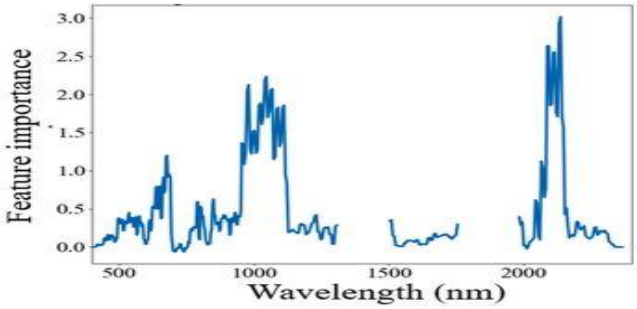

Figure 12. Predictive capabilities of each wavelength for CRC quantification (Wang et al. 2023).

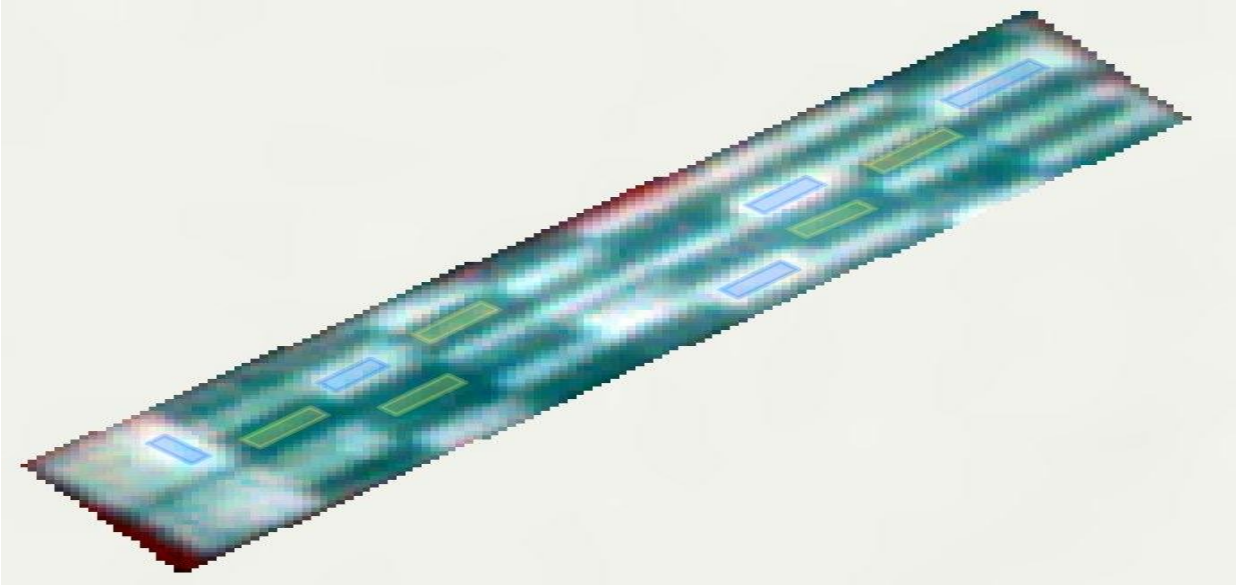

Figure 13. Delineation of areas with CRC marked in blue (n=5) and areas without CRC marked in yellow (n=5) in the research area, in the image dated August 10, 2022.

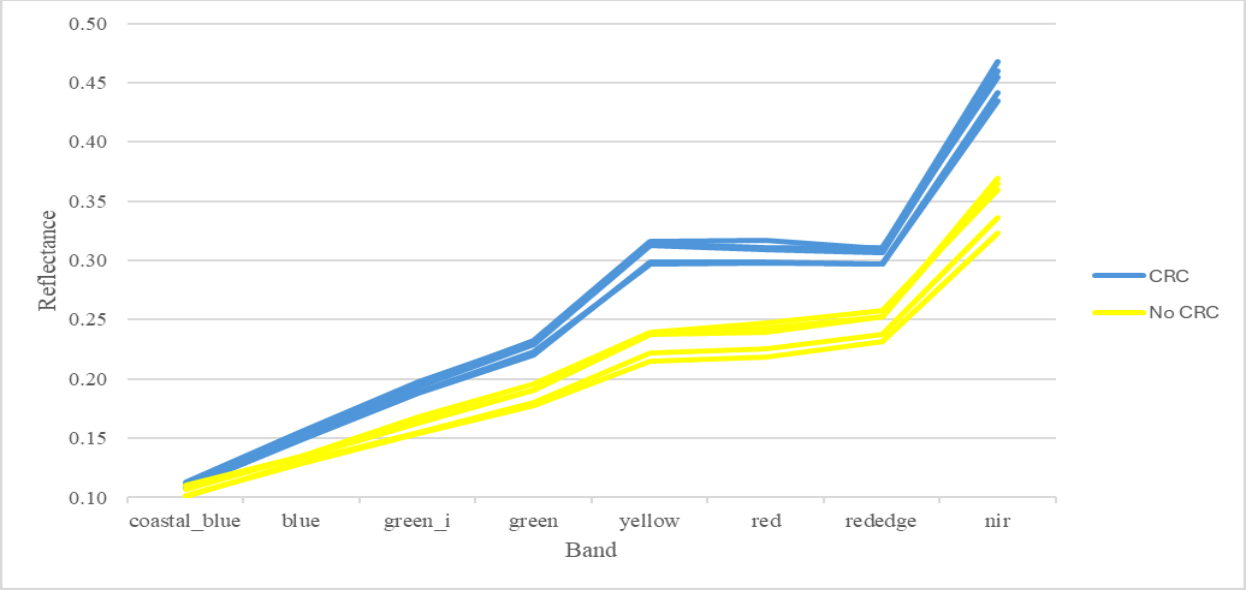

Figure 14. Spectral profile of areas with CRC marked in blue (n=5) and areas without CRC marked in yellow (n=5) in the research area, in the image dated August 10, 2022.

Considering the presented facts and examples, 16 spectral indices were formulated as candidates for the new crop residue index, proposed to be named the Normalized Difference Crop Residue Index (NDCRI), by leveraging four bands (yellow, red, red-edge, NIR) that exhibit high spectral reflectance in CRC locations and significant differentiation between areas with and without CRC on one side, four bands (coastal blue, blue, green_i, green) that show low spectral reflectance in CRC sites and minimal differentiation between areas with and without CRC on the other side. The

indices were developed using a normalized ratio between two bands (Table 4) to reduce variances in spectral response due to factors like lighting, shadows, surface texture, and atmospheric absorption (Sullivan et al., 2006).

Table 4. Candidate spectral indices for the Normalized Difference Crop Residue Index (NDCRI).

The New Crop Residue Index	Candidate Spectral Index for the New Crop Residue Index
The Normalized Difference Crop Residue Index (NDCRI)	(NIR-Coastal Blue)/(NIR+Coastal Blue)
	(NIR-Blue)/(NIR+Blue)
	(NIR-Green_i)/(NIR+Green_i)
	(NIR-Green)/(NIR+Green)
	(Red-Edge-Coastal Blue)/(Red-Edge+Coastal Blue)
	(Red-Edge-Blue)/(Red-Edge+Blue)
	(Red-Edge-Green_i)/(Red-Edge+Green_i)
	(Red-Edge-Green)/(Red-Edge+Green)
	(Red-Coastal Blue)/(Red+Coastal Blue)
	(Red-Blue)/(Red+Blue)
	(Red-Green_i)/(Red+Green_i)
	(Red-Green)/(Red+Green)
	(Yellow-Coastal Blue)/(Yellow+Coastal Blue)
	(Yellow-Blue)/(Yellow+Blue)
	(Yellow-Green_i)/(Yellow+Green_i)
	(Yellow-Green)/(Yellow+Green)

In addition, to minimize the influence of vegetation on the new CRC index, NDVI was calculated from the PlanetScope reflectance bands as:

$$NDVI=(NIR-Red)/(NIR+Red) \quad (1)$$

Since the practice of masking areas with significant green vegetation using the NDVI>0.3 condition had been already established for residue cover classification (Daughtry et al., 2004; Serbin et al., 2009a), the study, bypassing the green-up phase of winter wheat, focused on the phases of crop maturity and residue presence within the research field to prevent misclassification of mature winter wheat as residue. Accordingly, imagery from August 10, 2022, displaying crop

residue, was analyzed in conjunction with imagery from June 18, 2022, which corresponds to the peak maturity of winter wheat, to define a refined NDVI threshold for precise crop residue detection.

3.3 Calibration and Map Production

We did not split the dataset into training and testing in the study due to the small size of the research area and the limited number of field measurements (n=20). Instead, all samples served as training data for the image captured on the day the ground-based evaluations were conducted, while images of the study site and the entire district from other days functioned as testing data for the obtained results.

For each in-field sampling location, the GPS coordinates were georegistered with the PlanetScope surface reflectance imagery from August 10, 2022. Values corresponding to the various spectral indices, proposed as NDCRI, were extracted employing the Zonal Statistics geoprocessing tool in the Spatial Analyst toolbox of ArcGIS Desktop 10.8.2. Subsequently, CRC was graphed against each spectral index, leading to the formulation of correlation equations through both (a) simple linear regression and (b) second-degree polynomial regression. The most accurate spectral index from the two methods was selected as the new crop residue index, based on its goodness of fit (R^2) and root mean squared error (RMSE) values. To rigorously assess the performance of NDCRI, the study managed a series of statistical analyses including comparing measured versus predicted values, analyzing a residual, assessing normality with a Q-Q plot, and implementing both ordinary least squares (OLS) and random forest regressions, thereby providing a robust evaluation of its reliability and predictive accuracy for CRC measurement. Furthermore, by categorizing CRC into four levels (0–15%, 15–30%, 30–60%, and >60%) (CTIC, 2022) and utilizing an error matrix, we determined the overall accuracy and kappa coefficient of the novel indicator for the dataset. Significantly, all analyses were carried out using Python 3 software (Van Rossum & Drake, 2009). NDCRI, after being converted to single-band index values, was initially applied to imagery from August 10, 2022, and then extended to images of both the study area and the entire district on various days for mapping residue cover, employing ArcGIS Desktop 10.8.2. Moreover, NDVI was employed as a mask on PlanetScope surface reflectance images to concentrate analysis on areas devoid of vegetative ground cover.

CHAPTER 4: RESULTS AND DISCUSSION

4.1 In-Situ Sampling Results

The percentage of residue cover at the selected locations (n=20) varied between 3% and 97% (Figure 15 and Figure 16), predominantly consisting of winter wheat residue, with rice residue present in smaller amounts. The results at sample locations 6 and 17 were identical (both at 6%), while diverse outcomes were observed at the remaining observation sites. Despite endeavors to gather specimens from diverse sections of the study area, the findings were largely concentrated in two brackets, with seven samples falling within the 0-25% range and eight samples in the 75-100% range. It should be noted that the field experiment was conducted just two days after planting mung bean, resulting in virtually zero green vegetation cover in the research field.

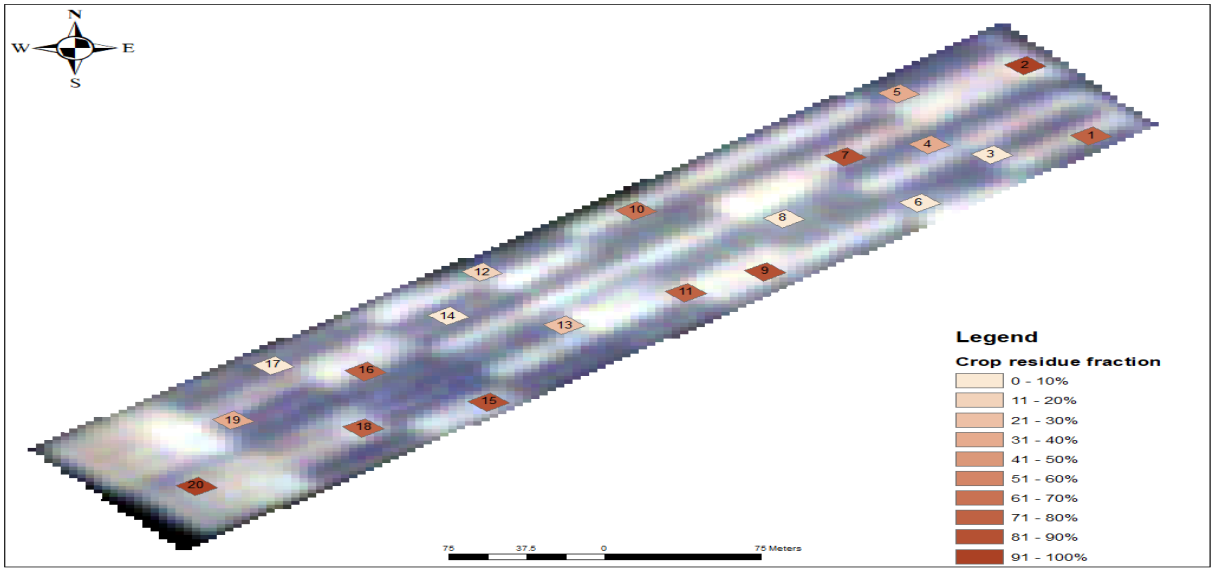

Figure 15. Percentage of residue cover at 20 sample locations in the research area, in the image dated August 10, 2022 (Note: Numbering of the sample locations begins corresponding to the starting point of the field).

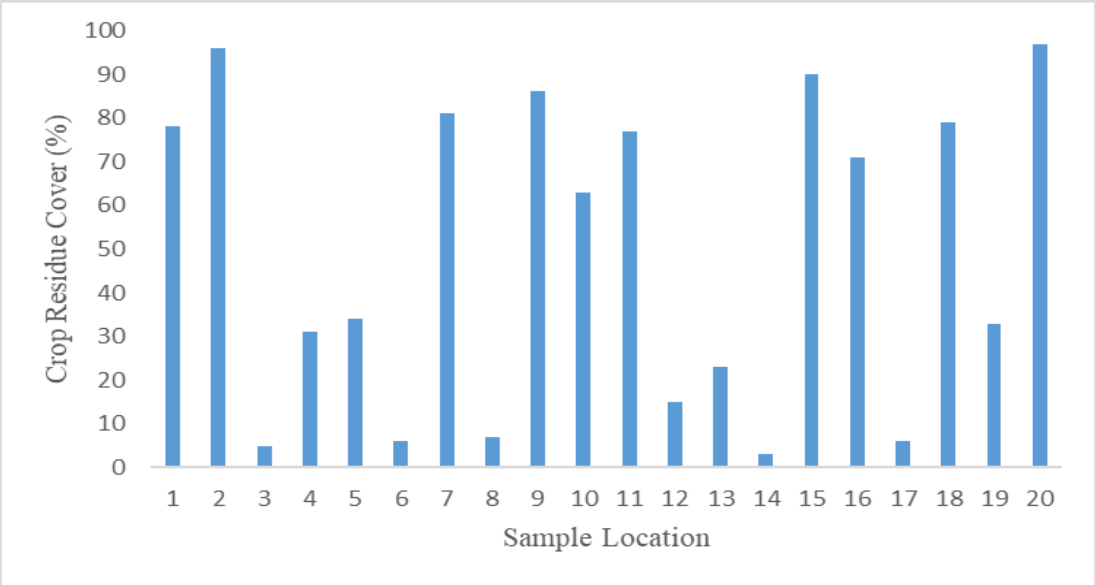

Figure 16. Percentage of residue cover at 20 sample locations in the research area, in the image dated August 10, 2022.

4.2 Metrics of Index Success

CRC measurements obtained from the field were compared to index values derived from imagery for each spectral index (Figure 17, Figure 18, Figure 19, and Figure 20). Upon applying both linear and second-order polynomial regression analyses to the comparisons, it was observed that second-order polynomial regressions invariably demonstrated superior R^2 values and minimized RMSE (Table 5). The data suggest a nonlinear relationship between the spectral indices and the CRC, with polynomial fits proving to be more reliable.

The correlation of all 16 indices with percent residue cover varied, as evidenced by R^2 values ranging from 0.078 to 0.6934 and RMSE values from 33.22 to 19.15 for the second-order polynomial fits (Table 5). Spectral indices incorporating red band typically surpassed indices using NIR, red-edge, and yellow bands in analogous band pairings regarding both coefficient of determination and residual error. Consequently, a (Red-Blue)/(Red+Blue) band combination, which displayed the highest R^2 (0.6934) and the lowest RMSE (19.15) (Table 5) among all the spectral indices in the second-order polynomial fit, was validated as the formula for the newly established crop residue index (NDCRI):

$$NDCRI=(Red-Blue)/(Red+Blue) \quad (2)$$

Table 5. Comparison of R^2 and RMSE values for first and second-order polynomial fits of candidate spectral indices for the new crop residue index (NDCRI) with field measurements (Note: The bold italic text represents the best spectral index performance).

The New Crop Residue Index	**Candidate Spectral Index for the New Crop Residue Index**	**R^2: 1st Order Full Range Linear Fit**	**R^2: 2nd Order Polynomial**	**RMSE: 1st Order Full Range Linear Fit**	**RMSE: 2nd Order Polynomial**
The Normalized Difference Crop Residue Index (NDCRI)	(NIR-Coastal Blue)/(NIR+Coastal Blue)	0.557	0.56	23.02	22.92
	(NIR-Blue)/(NIR+Blue)	0.463	0.52	25.34	23.96
	(NIR-Green_i)/(NIR+Green_i)	0.261	0.339	29.73	28.12
	(NIR-Green)/(NIR+Green)	0.174	0.195	31.44	31.03
	(Red-Edge-Coastal Blue)/(Red-Edge+Coastal Blue)	0.616	0.623	21.42	21.23
	(Red-Edge-Blue)/(Red-Edge+Blue)	0.6	0.601	21.88	21.83
	(Red-Edge-Green_i)/(Red-Edge+Green_i)	0.177	0.239	31.38	30.17
	(Red-Edge-Green)/(Red-Edge+Green)	0.0018	0.078	34.56	33.22
	(Red-Coastal Blue)/(Red+Coastal Blue)	0.677	0.692	19.64	19.2
	(Red-Blue)/(Red+Blue)	***0.691***	***0.6934***	***19.23***	***19.15***
	(Red-Green_i)/(Red+Green_i)	0.649	0.658	20.49	20.21
	(Red-Green)/(Red+Green)	0.552	0.554	23.14	23.09
	(Yellow-Coastal Blue)/(Yellow+Coastal Blue)	0.65	0.664	20.45	20.05
	(Yellow-Blue)/(Yellow+Blue)	0.622	0.65	21.25	20.46
	(Yellow-Green_i)/(Yellow+Green_i)	0.491	0.567	24.67	22.75
	(Yellow-Green)/(Yellow+Green)	0.482	0.53	24.88	23.7

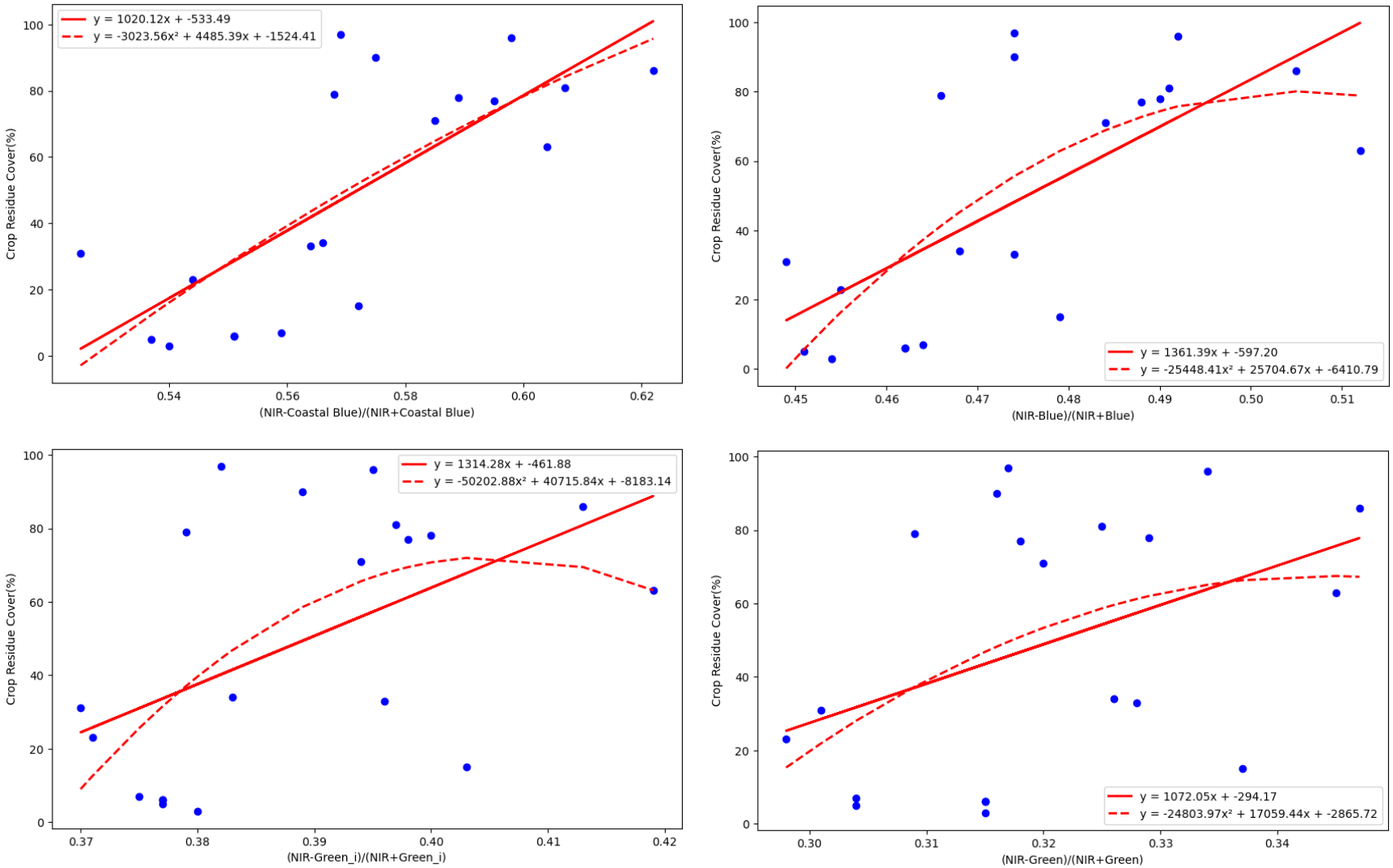

Figure 17. Correlation of CRC (%) with four NDCRI candidate spectral indices using linear (solid red line) and polynomial (dashed red line) regression models: (NIR-Coastal Blue)/(NIR+Coastal Blue), (NIR-Blue)/(NIR+Blue), (NIR-Green_i)/(NIR+Green_i), (NIR-Green)/(NIR+Green).

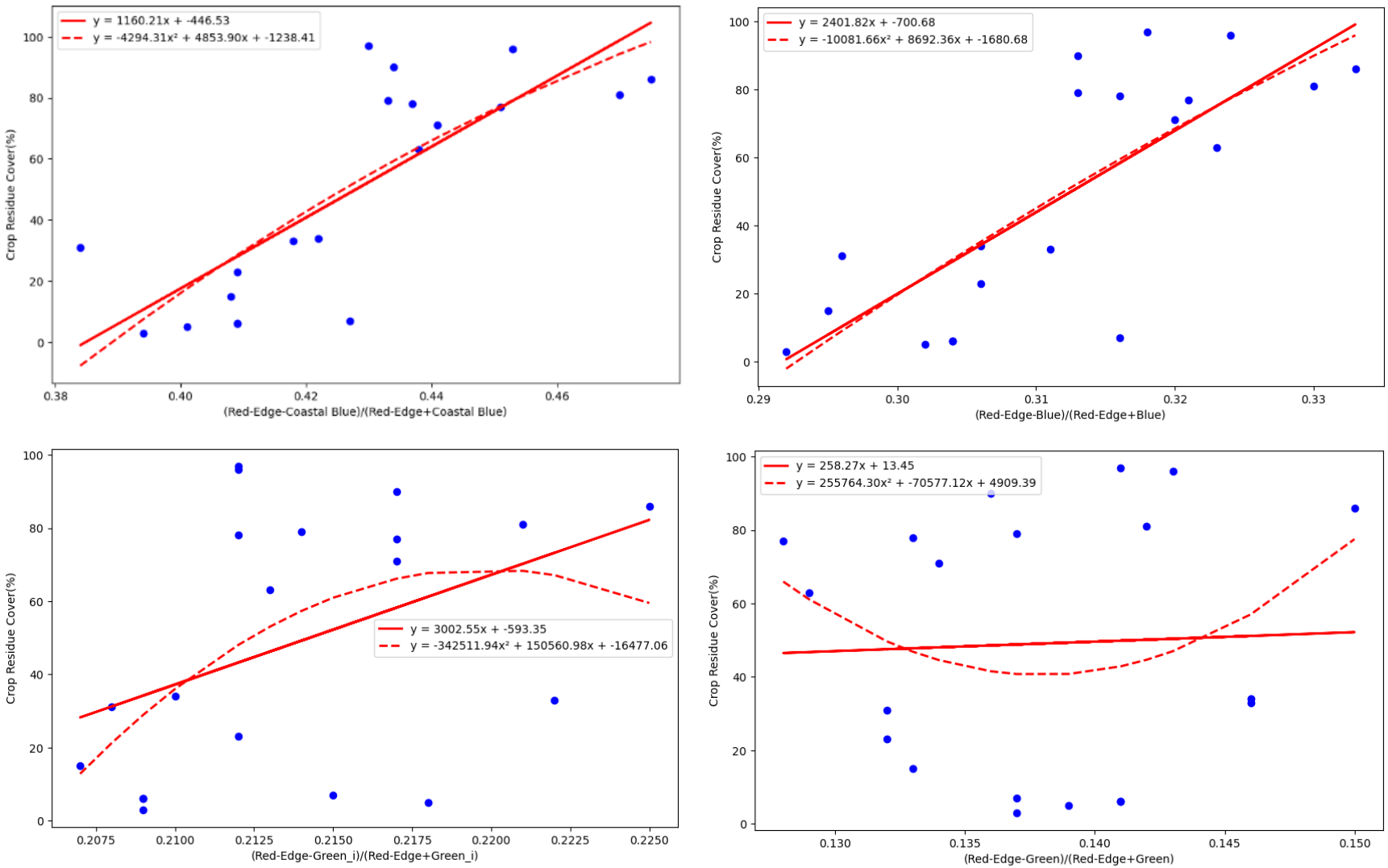

Figure 18. Correlation of CRC (%) with four NDCRI candidate spectral indices using linear (solid red line) and polynomial (dashed red line) regression models: (Red-Edge-Coastal Blue)/(Red-Edge+Coastal Blue), (Red-Edge-Blue)/(Red-Edge+Blue), (Red-Edge-Green_i)/(Red-Edge+Green_i), (Red-Edge-Green)/(Red-Edge+Green).

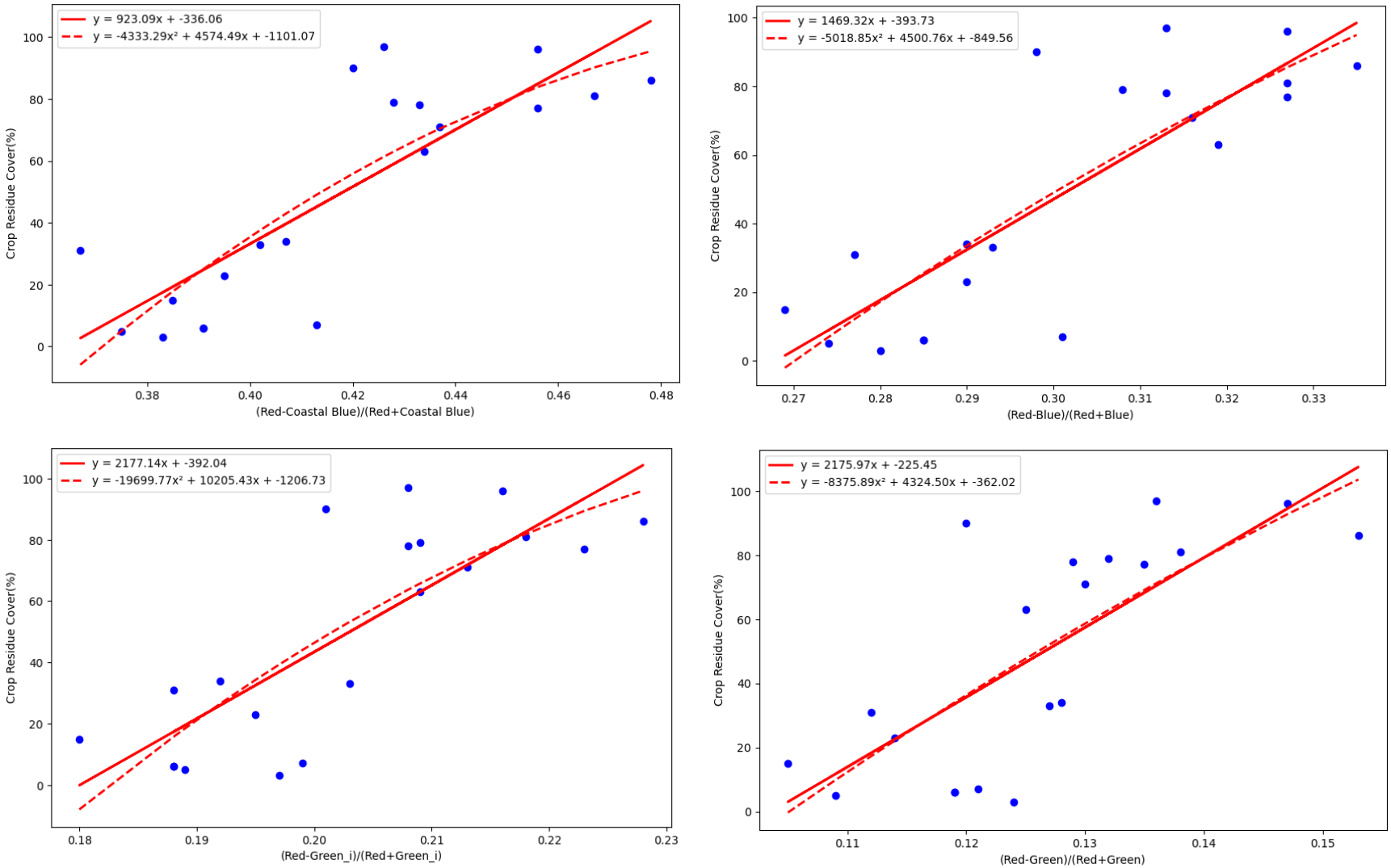

Figure 19. Correlation of CRC (%) with four NDCRI candidate spectral indices using linear (solid red line) and polynomial (dashed red line) regression models: (Red-Coastal Blue)/(Red+Coastal Blue), (Red-Blue)/(Red+Blue), (Red-Green_i)/(Red+Green_i), (Red-Green)/(Red+Green).

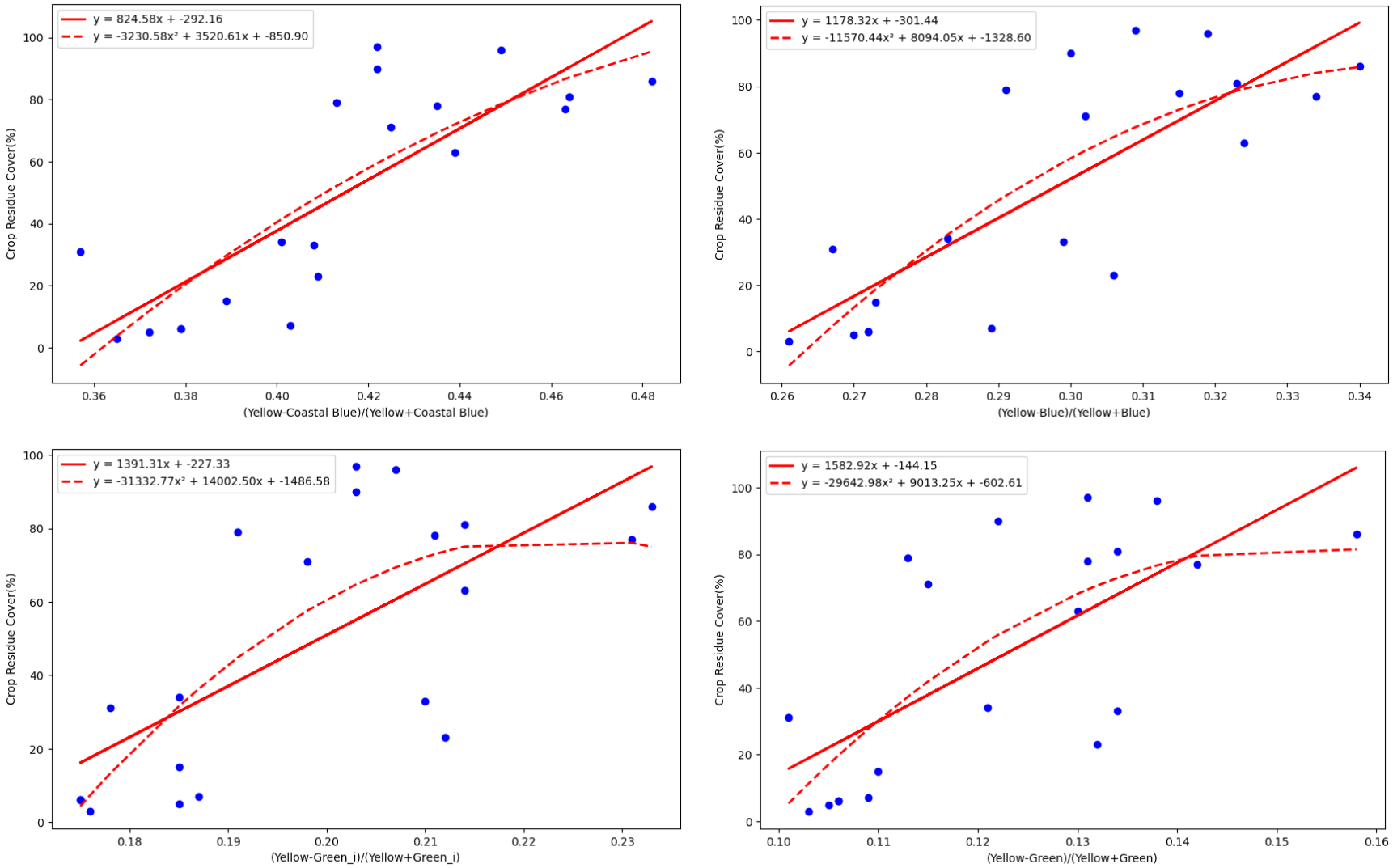

Figure 20. Correlation of CRC (%) with four NDCRI candidate spectral indices using linear (solid red line) and polynomial (dashed red line) regression models: (Yellow-Coastal Blue)/(Yellow+Coastal Blue), (Yellow-Blue)/(Yellow+Blue), (Yellow-Green_i)/(Yellow+Green_i), (Yellow-Green)/(Yellow+Green).

As an additional test, the study conducted comprehensive statistical evaluations of NDCRI's capability to monitor CRC using polynomial regression models, which encompassed residual analysis (Figure 21), normality checks via Q-Q plot (Figure 22), and the utilization of random forest (Figure 23) and OLS (Figure 24) regressions.

The distribution of residuals around the zero line (Figure 21) indicated some deviation from the ideal, reflecting that NDCRI may not capture all the variability within the dataset. The existence of residuals with notably large magnitudes pointed to limitations in the index's predictive accuracy for crop residue fraction in specific instances.

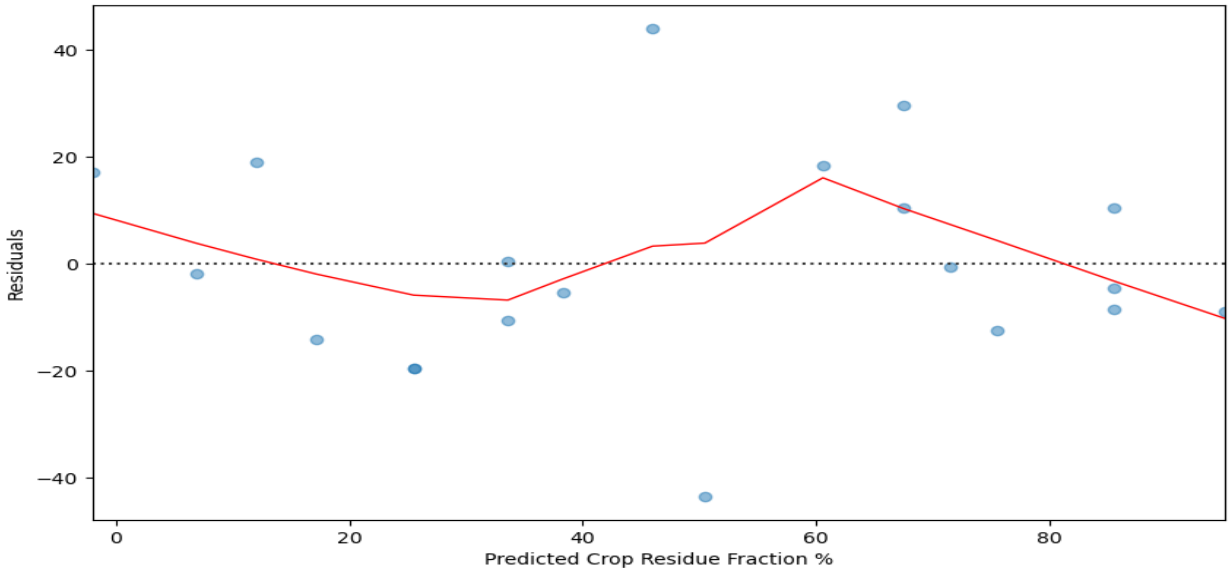

Figure 21. Residual analysis of polynomial regression for predicting crop residue fraction.

Selected instances notably diverged from the line in the Q-Q plot (Figure 22), particularly within the tails—more so on the left than the right—showing the potential presence of outliers or a distribution of residuals with heavier tails than a normal distribution. However, most data points aligned closely with the red line, especially at the center of the distribution, suggesting that the residuals from the polynomial regression were approximately normally distributed in the range.

It is important to note that the effectiveness of CRC practice depends on local conditions and requirements. Existing CRC strategies may not fully correspond to the specificities, thereby underscoring the necessity for innovative approaches. There is always an opportunity to investigate novel modifications to CRC policies, aiming to improve agriculture practices tailored to particular environmental settings.

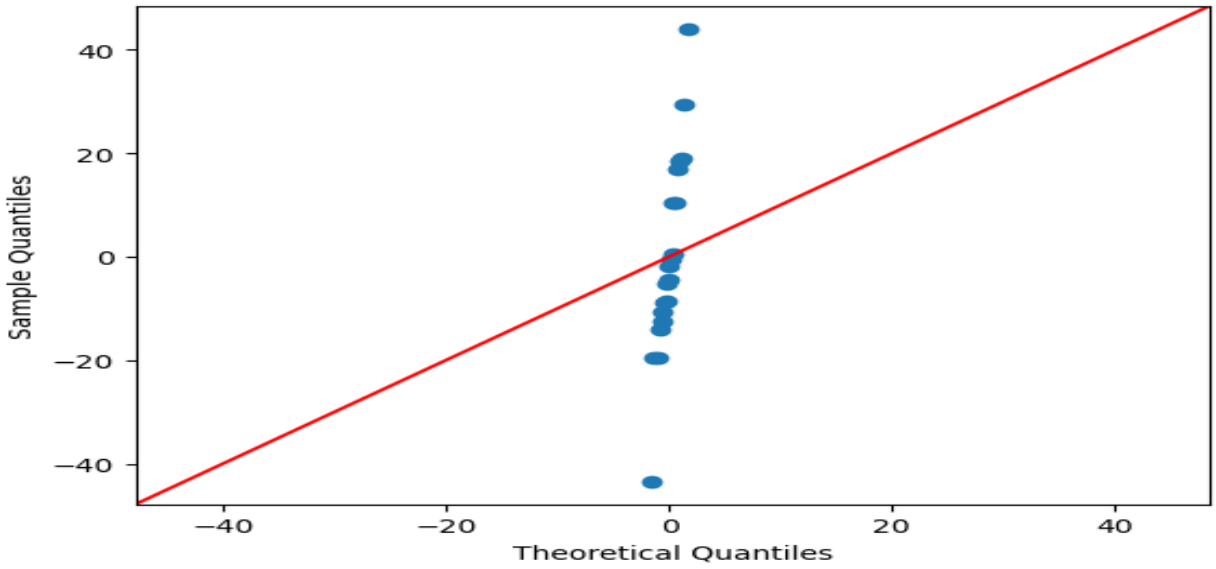

Figure 22. Q-Q plot for assessing normality of residuals in the polynomial regression model.

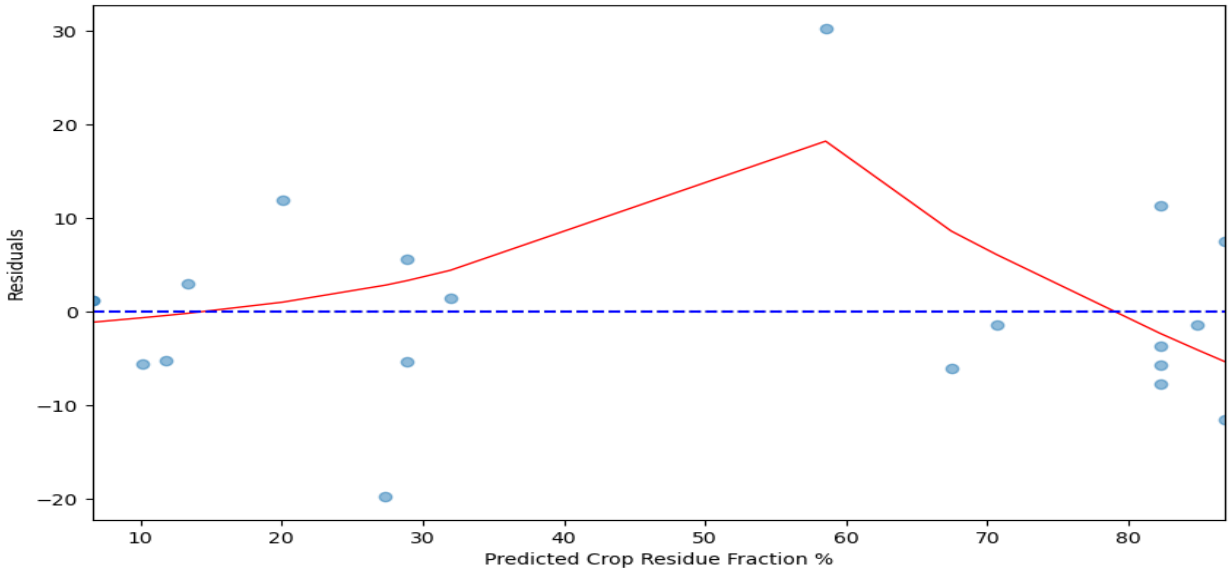

Figure 23. Residuals distribution for predicted crop residue fraction using random forest regression.

The OLS regression results (Figure 24) yielded an R^2 of 0.693, indicating that approximately 69.3% of the variability in crop residue fraction was captured by the index. The slight reduction to an adjusted R^2 of 0.657 took into consideration the number of predictors, which was expected given the index's complexity and sample size. The large standard errors associated with the coefficients may suggest a potential decrease in NDCRI's precision across different datasets or conditions. Nevertheless, the significant overall F-statistic confirmed the statistical validity of NDCRI. A

Durbin-Watson statistic close to 2.0 implied minimal residual autocorrelation, and the condition number did not raise concerns of severe multicollinearity, both of which bolster the index's robustness.

Dep. Variable:	CropResidueFraction	R-squared:	0.693
Model:	OLS	Adj. R-squared:	0.657
Method:	Least Squares	F-statistic:	19.23
Date:	Tue, 02 Apr 2024	Prob (F-statistic):	4.32e-05
Time:	10:46:03	Log-Likelihood:	-87.433
No. Observations:	20	AIC:	180.9
Df Residuals:	17	BIC:	183.9
Df Model:	2		
Covariance Type:	nonrobust		

	coef	std err	t	P>|t|	[0.025	0.975]
const	-849.5609	1272.306	-0.668	0.513	-3533.892	1834.771
x1	4500.7624	8451.181	0.533	0.601	-1.33e+04	2.23e+04
x2	-5018.8456	1.4e+04	-0.359	0.724	-3.45e+04	2.45e+04

Omnibus:	1.011	Durbin-Watson:	1.997
Prob(Omnibus):	0.603	Jarque-Bera (JB):	0.183
Skew:	0.191	Prob(JB):	0.912
Kurtosis:	3.272	Cond. No.	3.70e+03

Figure 24. OLS regression results for evaluating the predictive performance of the crop residue index.

The statistical analyses presented a nuanced view of the new index. While the OLS regression showcased a respectable R^2, indicating a strong explanatory power, the magnitude of residuals in both the polynomial and random forest regressions suggested some predictive limitations in certain cases. Nonetheless, the lack of systematic patterns in the residuals and the approximate normal distribution, particularly noted in the central range of the Q-Q plot, signaled that NDCRI generally models the variability in crop residue fraction effectively. The overall positive performance, coupled with the statistical significance of the index, supported NDCRI's utility as a viable index for estimating CRC.

Furthermore, we found a linear relationship between measured and predicted CRC with an R^2 of 0.46 and RMSE of 25.31% (Figure 25) and constructed an error matrix (Table 6) for the four residue cover categories (0–15%, 15–30%, 30–60%, and >60%) with the overall accuracy 60% and the Kappa coefficient 42% for the dataset. While the moderate results denoted the new index tend to overestimate residue in low-residue areas, likely due to the soil's spectral influence, it also showed that NDCRI is responsive and able to differentiate residue levels effectively. The observed pattern demonstrated its potential as a valuable tool for detecting CRC, especially with further refinement to reduce soil spectral interference.

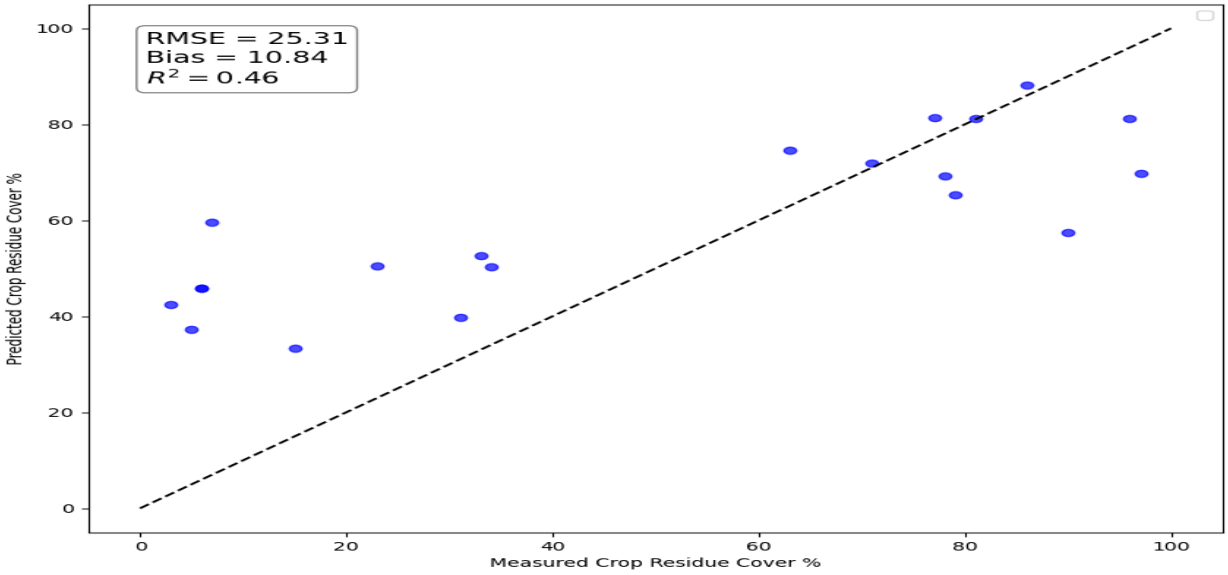

Figure 25. Measured vs predicted CRC for the dataset.

Table 6. Error matrix for four residue cover classes for the dataset (Note: The bold italic text represents the number of pixels correctly assigned to each class).

Classification Data		**Reference Data**				
	CRC<15 %	15%<CRC<30 %	30%<CRC<60 %	CRC>60 %	Total	User Accuracy
CRC<15%	***0***	0	5	0	5	0%
15%<CRC<30 %	0	***0***	2	0	2	0%
30%<CRC<60 %	0	0	***3***	0	3	100%
CRC>60%	0	0	1	***9***	10	100%
Total	0	0	11	9	20	
Producer Accuracy	0%	0%	27%	100%		
Overall accuracy: 60%						
Kappa coefficient: 42%						

Although the comparison result of the new index with the ground measurements was not perfect (R^2=0.6934), it outperformed both CRC and Landsat-based NDTI (R^2=0.11) as reported by Daughtry et al. (2006), convolutional neural network (CNN) deep learning outcome, which achieved an R^2 of 0.91 with field measurements, and airborne-based NDTI (R^2=0.37), CAI (R^2=0.67) as recorded by Wang et al. (2023). Additionally, the same study by Wang et al. (2023) noted an R^2 of 0.22 when comparing ground-measured residue cover with satellite-measured residue cover from Landsat and Sentinel along a 1:1 line, whereas our study observed the figure to be 0.46. Only by incorporating airborne data and utilizing an upscaling approach from ground to airborne to satellite was the result elevated to an R^2 of 0.67 (Wang et al., 2023). Notably, earlier research has often categorized CRC into two or three segments to enhance the precision of their predictions (Gowda et al., 2001; Thoma et al., 2004; Zheng et al., 2012; Hively et al., 2018).

The performance of the new index, despite not achieving perfection, demonstrated an advancement in CRC assessment. By surpassing traditional methods and showcasing improved accuracy over existing satellite-based indices, it highlighted the potential of using higher-resolution PlanetScope data even without SWIR bands, which had been considered crucial for accurate CRC detection in previous studies. The findings suggested that NDCRI, with further calibration and refinement, could serve as a robust tool for agricultural management and conservation practices.

4.3 Vegetation Impact on Crop Residue Index Performance

Given the already established method of excluding areas with prominent green vegetation using an NDVI>0.3 threshold for classifying residue coverage (Daughtry et al., 2004; Serbin et al., 2009a), the research focused not on the green-up phase of winter wheat but on the critical periods of crop maturity and residue presence in the study area. The approach was adopted to avoid incorrectly identifying mature winter wheat as crop residue. Consequently, the image from August 10, 2022, showing crop residue, was examined together with the image from June 18, 2022, the period of winter wheat's highest maturity, to determine an adjusted NDVI threshold for accurate identification of crop residue.

NDVI values were extracted utilizing the Zonal Statistics geoprocessing tool in the Spatial Analyst toolbox of ArcGIS Desktop 10.8.2 for each in-field sampling location from imagery dated August 10, 2022. Since the percentage of residue cover at the selected locations (n=20), as determined through field measurements, ranged between 3% and 97%, it was posited that, barring any

anomalies, the NDVI readings for the observation sites would be representative of the entire area. Subsequently, CRC values were plotted against the determined NDVI values to analyze the achieved outputs. The results revealed that, excluding two outliers (which displayed significantly different values from the others), the NDVI measures for the remaining 18 locations fell between 0.190 and 0.215 (Figure 26). Therefore, it was concluded that within our area covered from minimal to maximal residue, the condition NDVI<0.215 could be applied to assess CRC.

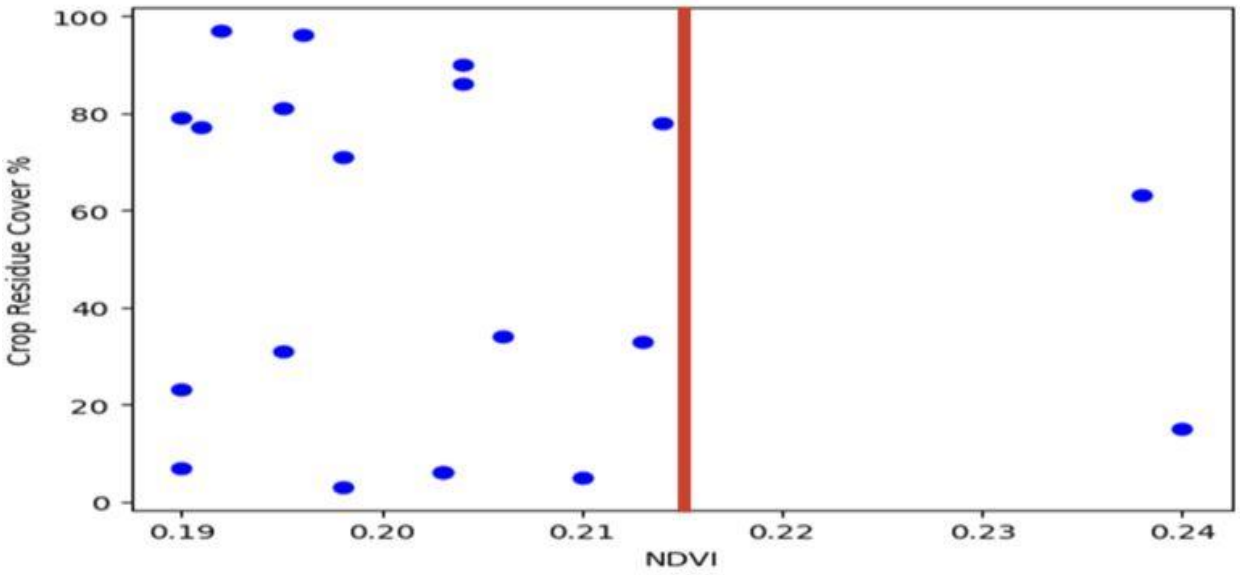

Figure 26. Scatter plot demonstrating the relationship between NDVI values and CRC percentages, with a vertical line indicating the proposed NDVI threshold for residue classification, in the image dated August 10, 2022.

Due to field measurements were not performed on the day the image was captured, June 18, 2022, NDVI data were ascertained for the whole study site. Afterward, almost the entire area was demarcated with the special polygon (Figure 27), leading to the creation of the unified spectral box (Figure 28) for the field's NDVI values employing ArcGIS Pro 3.0.0 software. The findings indicated that, with the exception of a few outliers presenting markedly divergent values, the NDVI levels for the majority of locations spanned from 0.223 to 0.256. Hence, it was deduced that within our study area, characterized by mature winter wheat, the NDVI measures were consistently above 0.223.

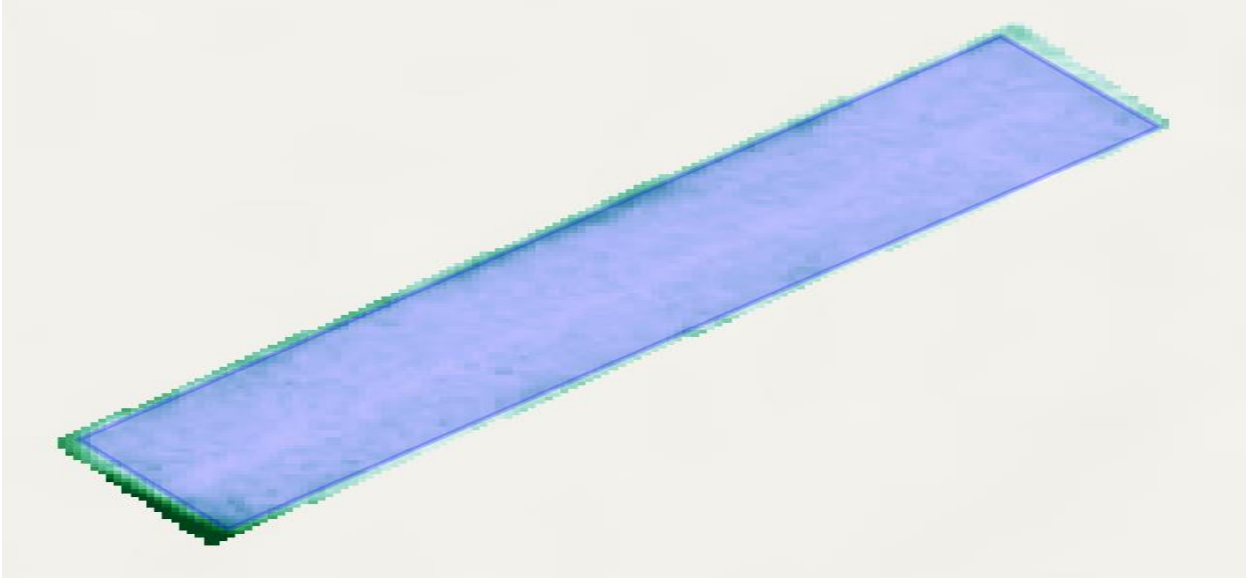

Figure 27. Delineation of the research area after NDVI calculation in mature winter wheat period, in the image dated June 18, 2022.

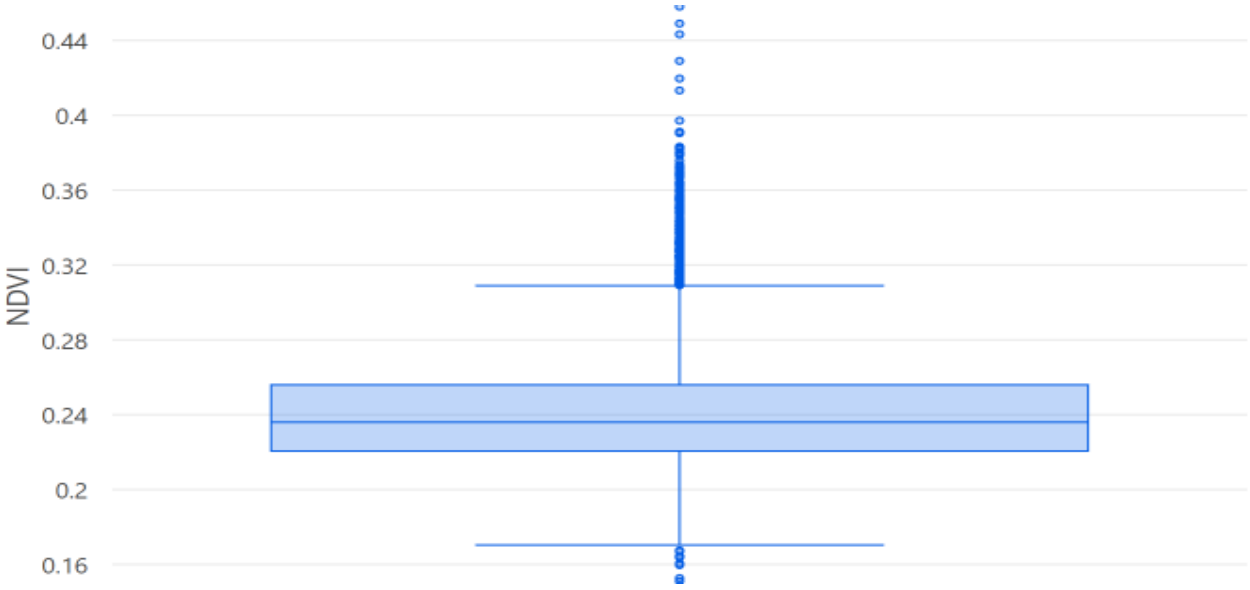

Figure 28. Boxplot of NDVI value distribution for the study area in mature winter wheat period, in the image dated June 18, 2022.

From the analysis of both images, a general conclusion was reached to harmonize the observations: NDVI values fall below 0.215 during the crop residue period and exceed 0.223 in the mature winter wheat phase. Accordingly, for a consistent approach in evaluating CRC, it was resolved to apply a threshold of NDVI<0.22. Similarly, for mapping purposes using the new crop residue index,

areas with vegetation were masked by adopting a threshold of NDVI>0.22, ensuring the exclusion of vegetated regions and focusing on residue-covered areas.

The key advancement from the analysis was that while the original NDVI threshold could only mask areas with substantial green vegetation (thus, sometimes misclassifying mature crops as residue), the updated NDVI threshold provided the capability to mask both areas with significant greenery and fields at various stages of crop maturity. The enhancement enabled a more accurate assessment of CRC, ensuring that mature crops were not erroneously classified as residue, thereby refining the accuracy of crop residue mapping.

4.4 Geospatial Representation of Crop Residue

Prior to the utilization of the novel crop residue index for cartographic representation, it was imperative to convert the index values into percentage terms. Initially, NDCRI was computed for the study area based on the August 10, 2022, imagery (Figure 30), which served as the primary dataset. The examination of the histogram (Figure 29) from the derived index values indicated a range predominantly between 0.23 and 0.35. To facilitate a standardized assessment of residue cover, the value of 0.23 was designated to represent a residue cover of 0%, and conversely, a value of 0.35 was determined to signify a full residue cover of 100%. The analysis laid the foundation for converting NDCRI values into percentages through the application of the following formula:

$$\text{Percentage} = \left(\frac{\text{"}NDCRI\,Raster\text{"} - 0.23}{0.35 - 0.23}\right) \times 100 \tag{3}$$

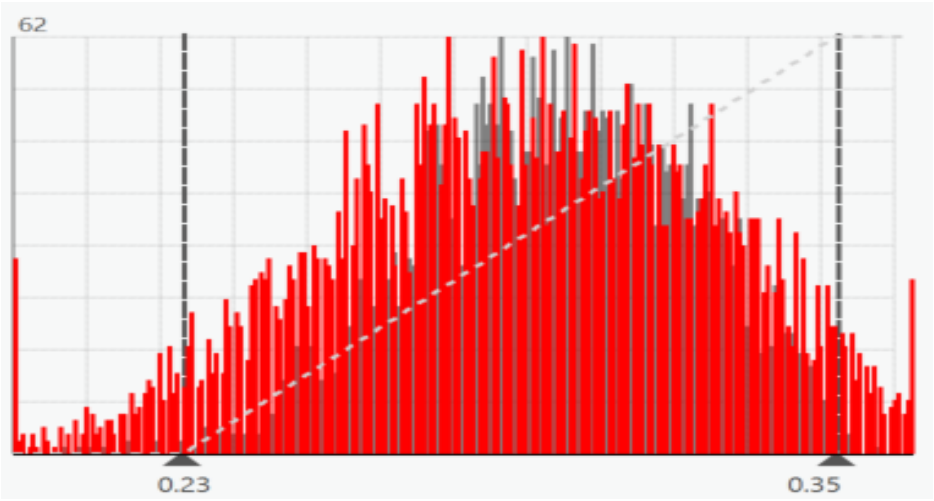

Figure 29. Histogram of NDCRI values across the study area.

Subsequent application of the conversion method to imagery from other dates yielded percentage representations of NDCRI. Importantly, for comparative analysis of residue indicators across the research field and district, the established reference values for 0% and 100% residue cover were consistently applied to all further images.

Temporal analysis was conducted to corroborate the NDCRI findings, employing five images captured on various dates—August 4, 2022 (Figure 31); July 7, 2022 (Figure 32); June 18, 2022 (Figure 33); May 12, 2022 (Figure 34); and March 2, 2022 (Figure 35)—corresponding to different stages in the crop cycle, as detailed in Table 2. Moreover, five additional images—August 6, 2022 (Figure 36); July 8, 2022 (Figure 37); June 18, 2022 (Figure 38); June 2, 2022 (Figure 39); and May 12, 2022 (Figure 40)—encompassing the entire Urtachirchik District, were utilized to validate the applicability of the index across a broader area. It is noteworthy that for the classification of residue cover, all regions exhibiting an NDVI value greater than 0.22 were masked to minimize the influence of vegetation on the residue detection process.

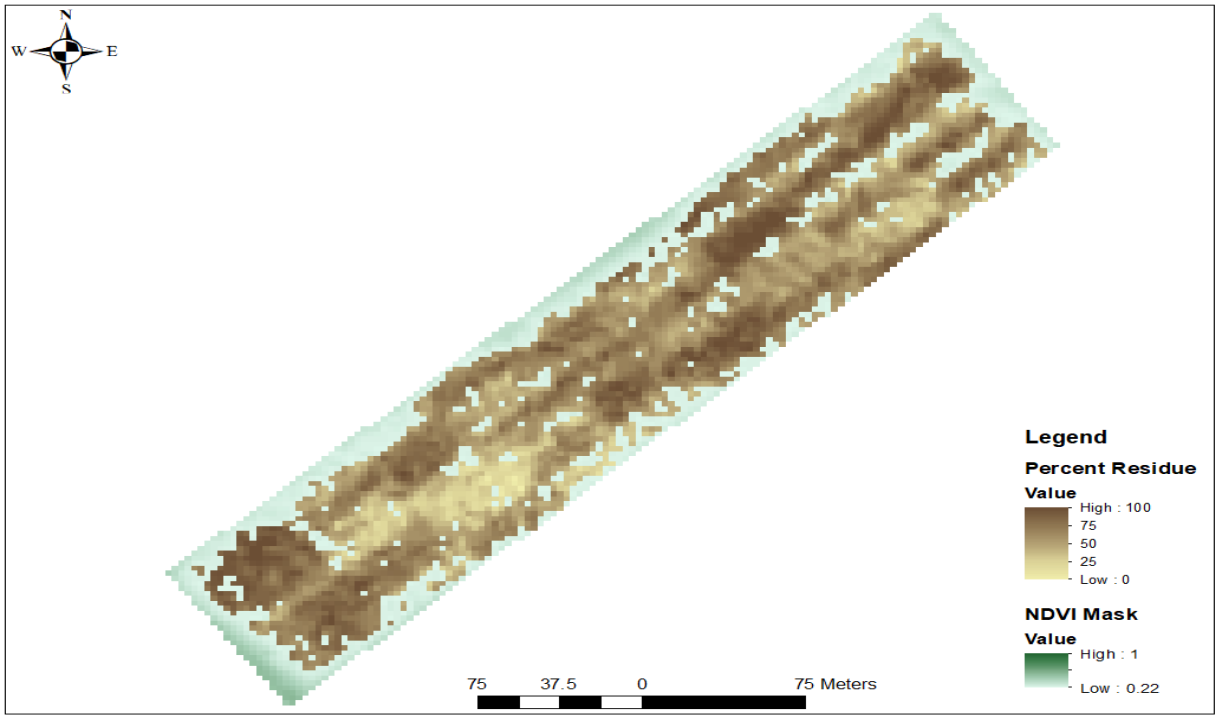

Figure 30. Map of CRC percentage with NDVI masking in the study area on August 10, 2022, using PlanetScope data.

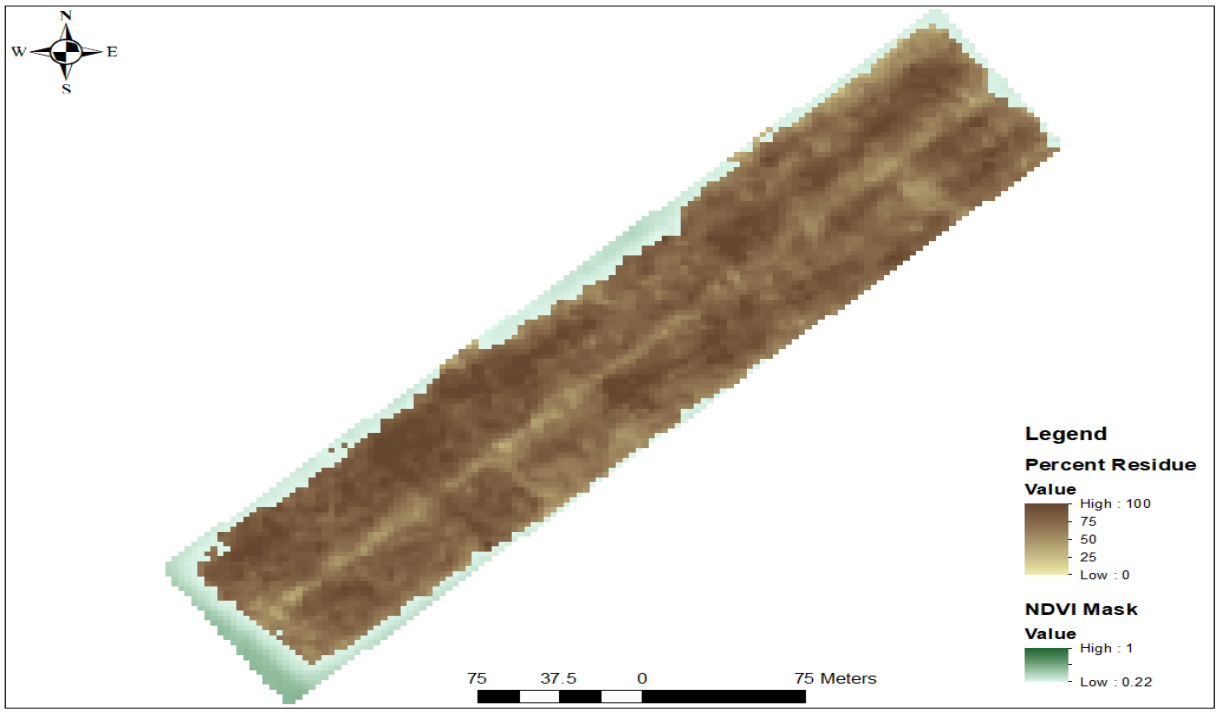

Figure 31. Map of CRC percentage with NDVI masking in the study area on August 4, 2022, utilizing PlanetScope data.

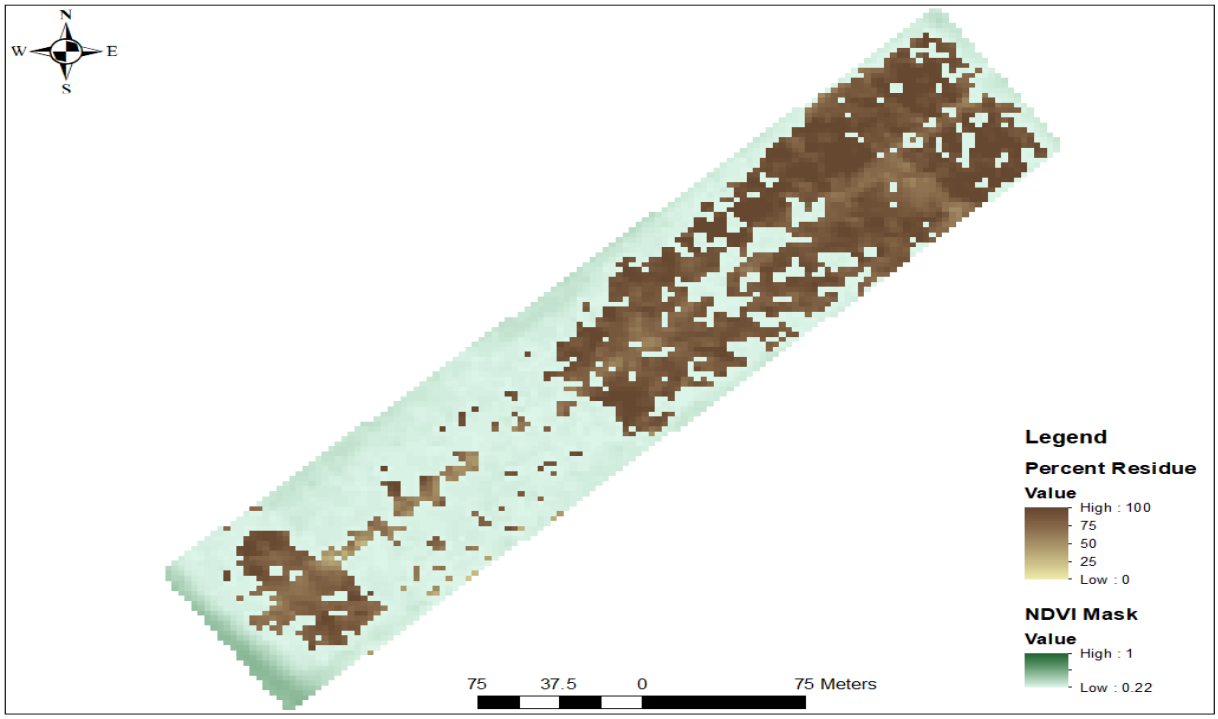

Figure 32. Map of CRC percentage with NDVI masking in the study area on July 7, 2022, employing PlanetScope data.

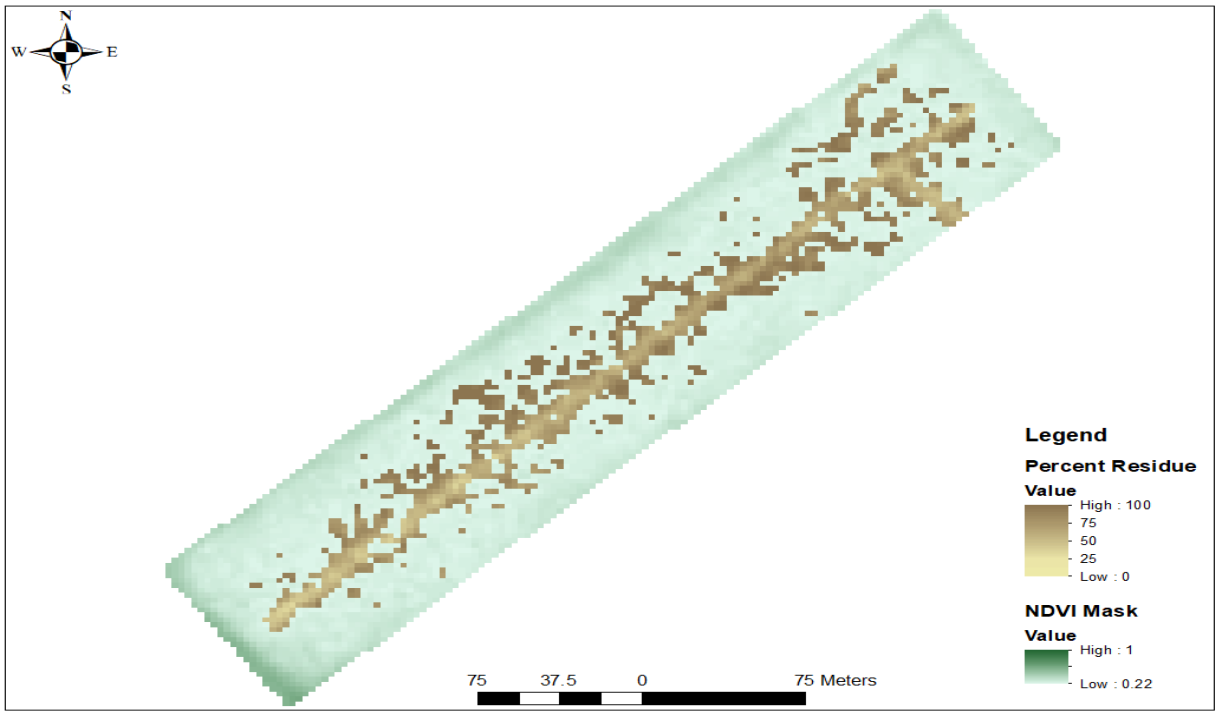

Figure 33. Map of CRC percentage with NDVI masking in the study area on June 18, 2022, applying PlanetScope data.

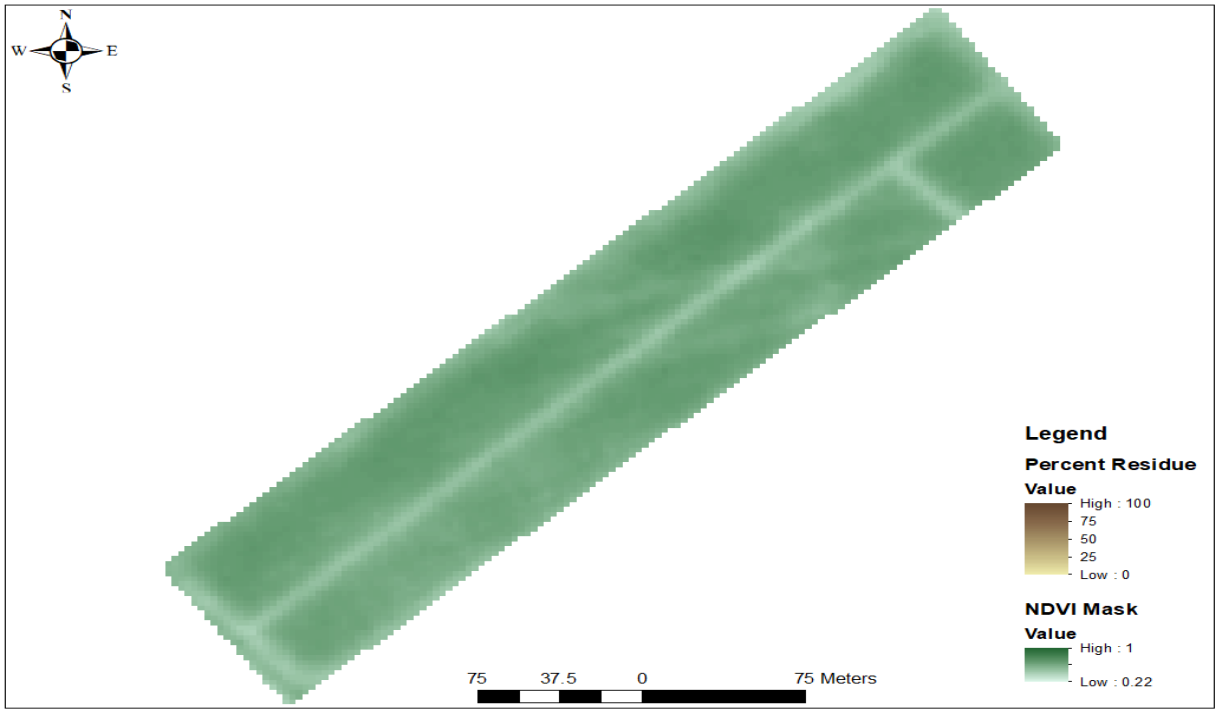

Figure 34. Map of CRC percentage with NDVI masking in the study area on May 12, 2022, leveraging PlanetScope data.

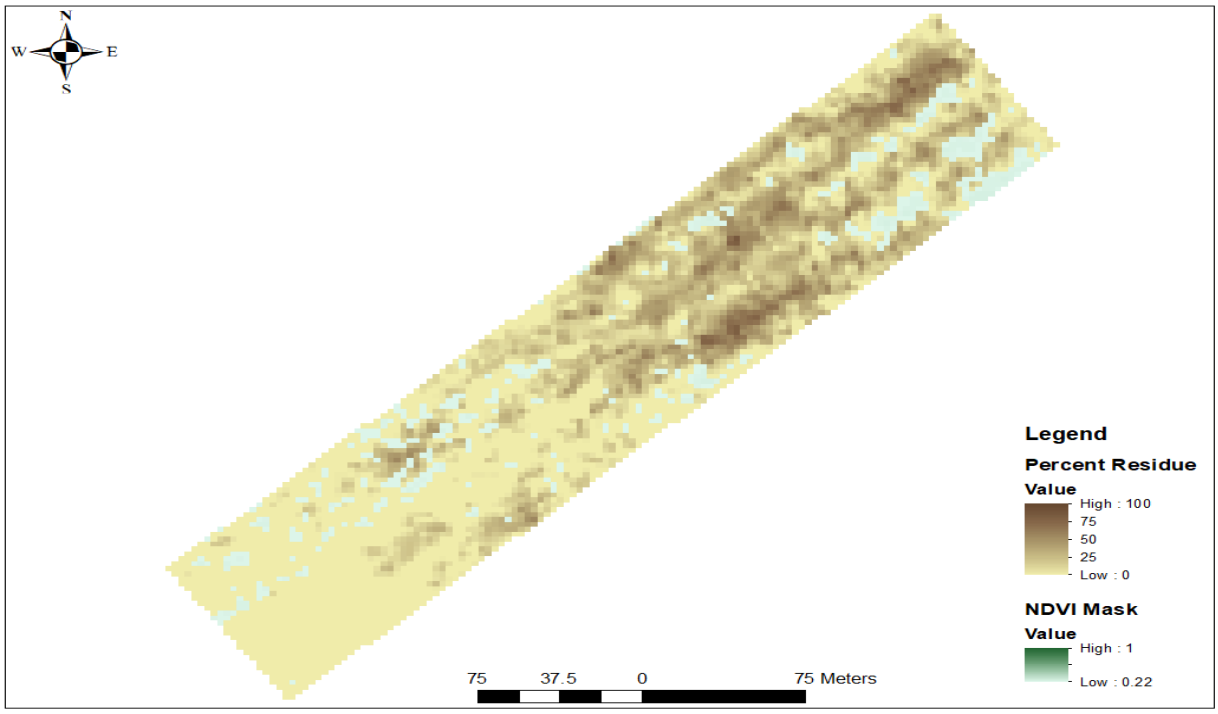

Figure 35. Map of CRC percentage with NDVI masking in the study area on March 2, 2022, operating PlanetScope data.

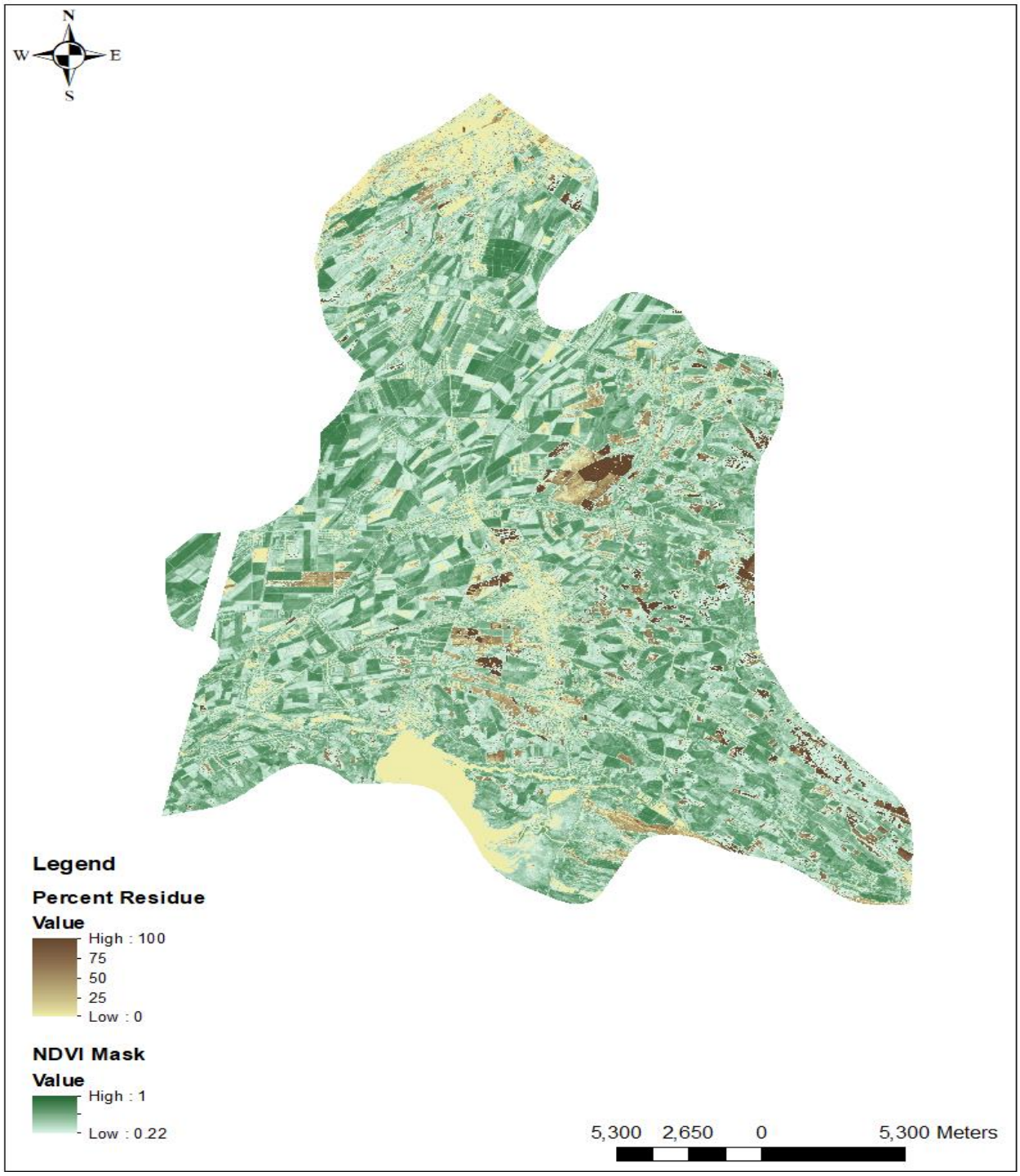

Figure 36. Map of CRC percentage with NDVI masking in the Urtachirchik District on August 6, 2022, using PlanetScope data.

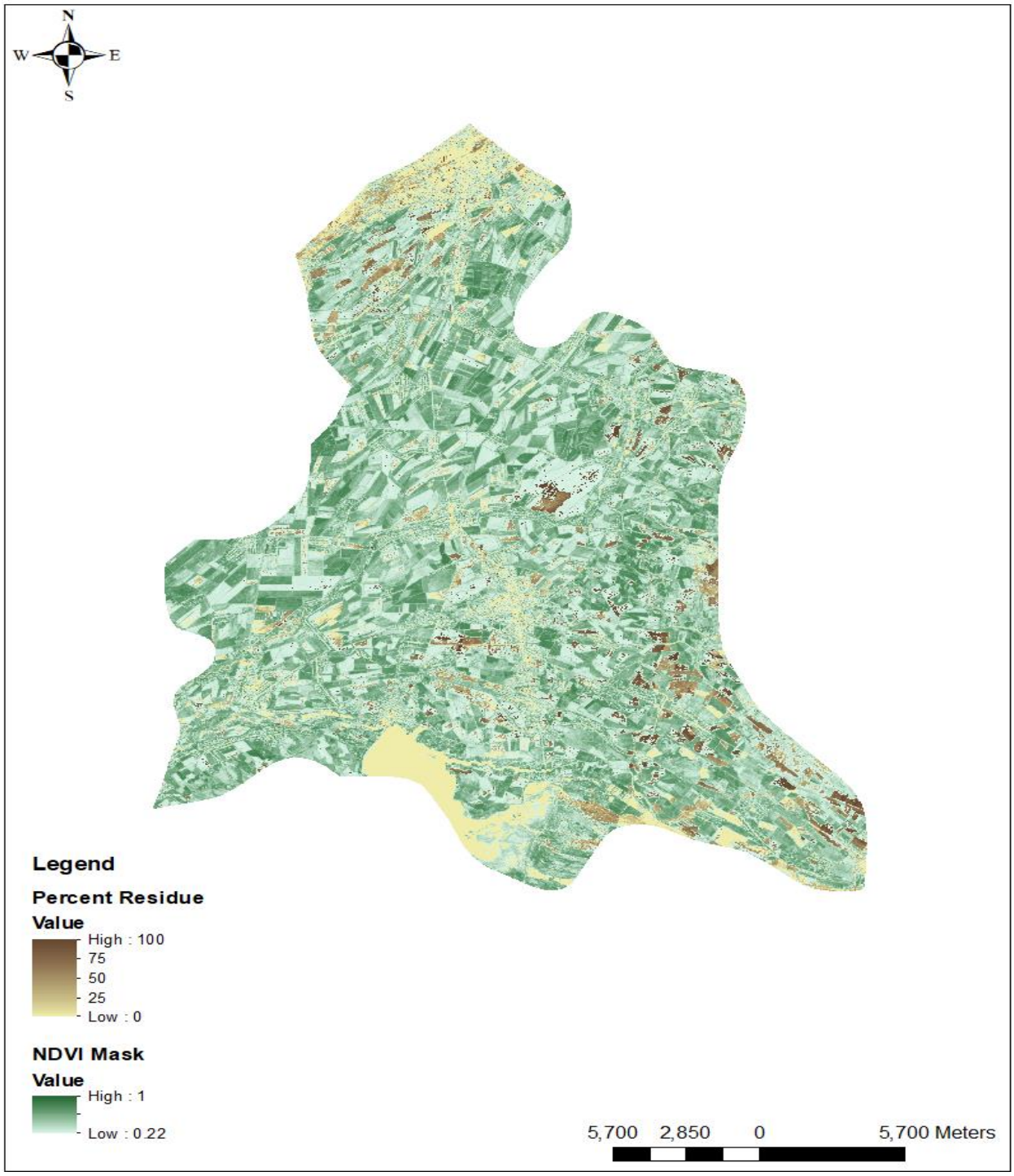

Figure 37. Map of CRC percentage with NDVI masking in the Urtachirchik District on July 8, 2022, utilizing PlanetScope data.

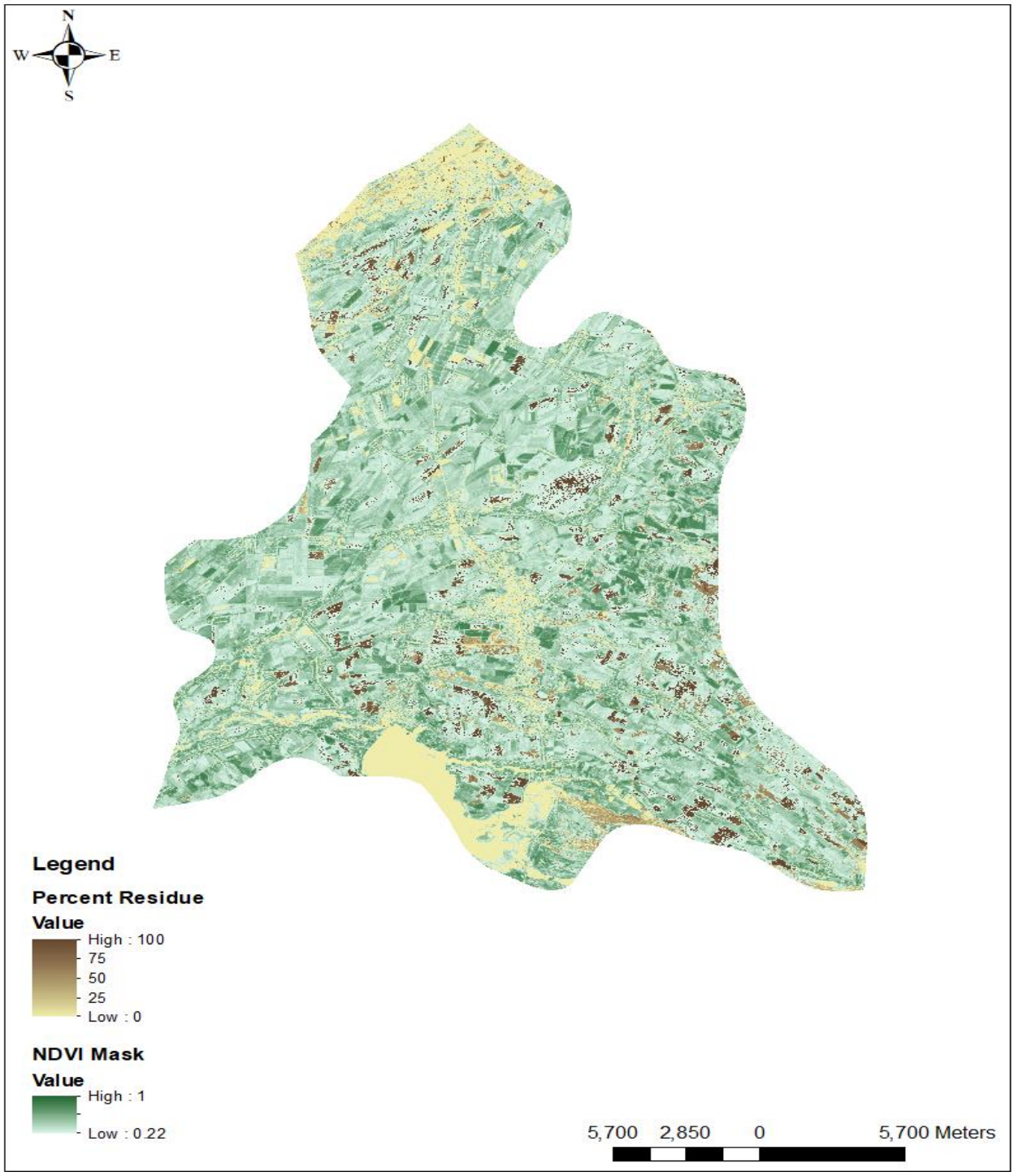

Figure 38. Map of CRC percentage with NDVI masking in the Urtachirchik District on June 18, 2022, employing PlanetScope data.

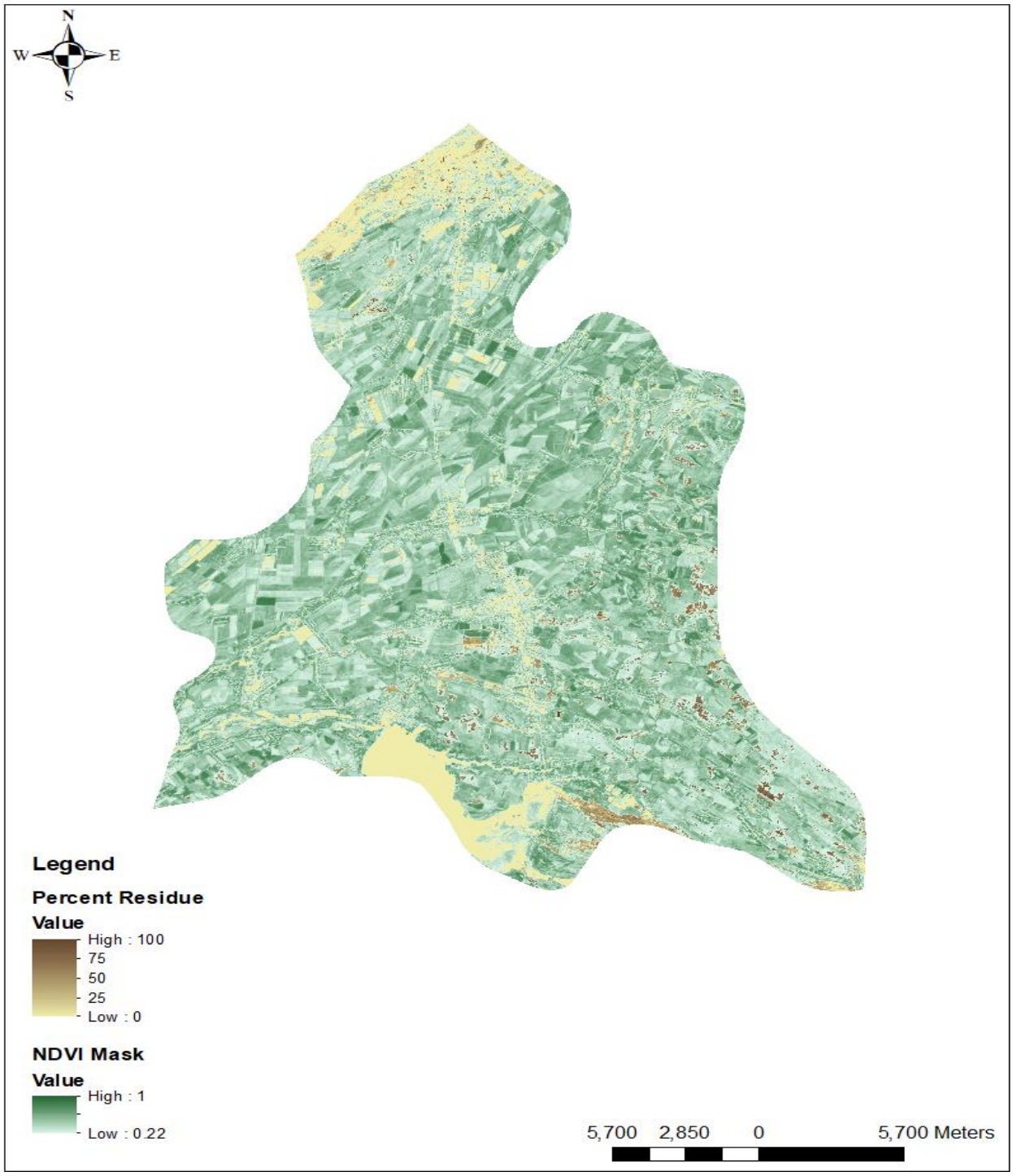

Figure 39. Map of CRC percentage with NDVI masking in the Urtachirchik District on June 2, 2022, applying PlanetScope data.

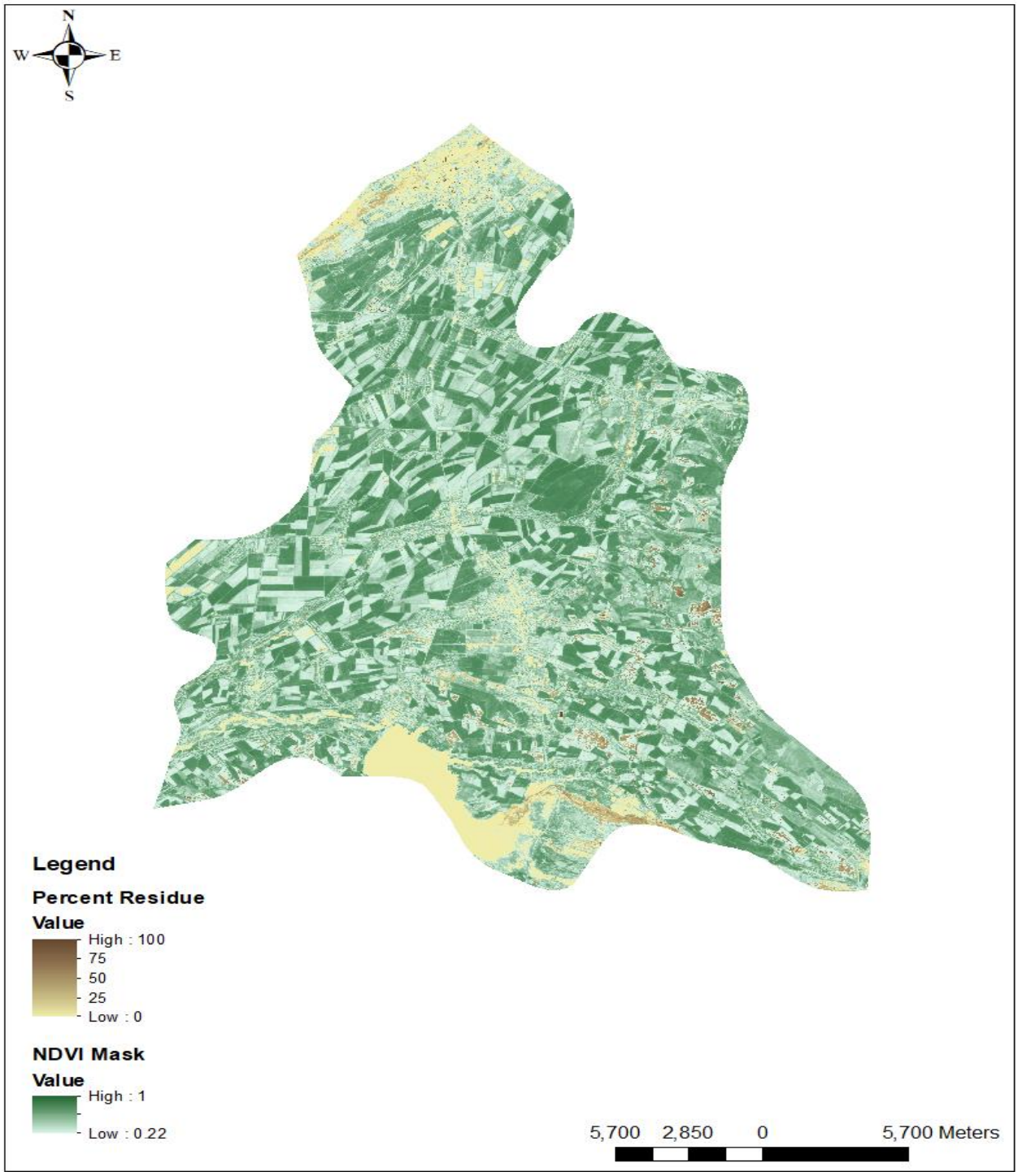

Figure 40. Map of CRC percentage with NDVI masking in the Urtachirchik District on May 12, 2022, leveraging PlanetScope data.

The analysis of maps from different dates indicated that soil and vegetation factors could influence the accuracy of CRC detection. For instance, on August 10, 2022, even though CRC and non-CRC areas were distributed fairly uniformly within the research field, the map (Figure 30) depicted higher percentages of residue in certain areas that did not contain CRC. Moreover, the layout dated June 18, 2022 (Figure 33), identified crop residue in regions of the area, although the fact that the winter wheat was in its maturity stage and had not yet been harvested. However, it was important to highlight that utilizing the revised NDVI threshold effectively minimized the misclassification of mature crops as residue, underscoring the employment of the method in enhancing the accuracy of crop residue detection.

The maps created during the study generally conformed to anticipated patterns. Specifically, the layout from August 4, 2022 (Figure 31), accurately represented the research area before any conservation or tillage practices had been applied, showing the field completely covered with crop residue. The maps from July 7 (Figure 32) and May 12 (Figure 34), 2022, illustrated the site at different stages of the crop cycle; the July layout captured the start of the harvest, revealing half the field covered with residue, while the May map displayed no residue, corresponding with the winter wheat's green-up phase. Noteworthy was the map from March 2, 2022 (Figure 35), which successfully quantified rice residue transported from another location. It indicated the new index's effectiveness in monitoring not just crop residue from cultivated fields but also residue relocated from elsewhere.

Given the national agricultural timeline indicating winter wheat planting in parts of the district similar to the research area, the maps generated for the Urtachirchik District showed no significant discrepancies. During times characterized by a minimal likelihood of crop residue presence, notably in the mappings from May 12 (Figure 40) and June 2 (Figure 39), 2022, CRC was scarcely detected. In contrast, at intervals marked by an elevated potential for CRC, such as depicted in the layouts from June 18 (Figure 38), July 8 (Figure 37), and August 6 (Figure 36), 2022, some portions of the district were markedly enveloped in CRC.

The findings, supported by PlanetScope's comprehensive coverage, illustrated the effectiveness of the new index in accurately representing both the presence and absence of crop residue across varied temporal stages, emphasizing its promise as a reliable instrument for agricultural management and environmental conservation efforts, subject to additional fine-tuning and adjustments.

4.5 Suggestions, Limitations, and Future Prospects

Suggestions

In accordance with FAO guidelines on CA (2024), the term "CRC" is typically applied to residue from crops cultivated within the same area. In our study conducted in the designated research field, we embarked on an experiment by transferring residue from different fields to assess its impact on the yield of the winter wheat crop and as an augmentative measure for initiating CA practices post-crop cycle. The outcomes showed that sub-fields supplemented with transported rice residue, where TA practices were integrated, manifested an approximate 15% increase in winter wheat yield in comparison to sub-fields devoid of such residue (Pulatov, in press). Moreover, post-harvest laboratory examinations unveiled that winter wheat spikes in residue-enriched sub-fields exhibited superior quality over non-residue areas (Pulatov, in press). Additionally, undecomposed rice residue after the winter wheat harvest facilitated an increased production of residues conducive to CA practices. Importantly, the newly developed index demonstrated its capacity not merely for monitoring residue from in-situ cultivated crops but also for residues relocated from disparate fields.

As mentioned before, the FAO's guidelines on CA (2024) highlight three core principles: minimal soil disturbance, continuous organic soil cover, and crop diversification. The guidelines advocate for adaptations to accommodate specific local conditions and needs. A common challenge faced by many local farmers involves the difficulty of sowing new crops in fields blanketed with crop residue, constrained by the capabilities of available agricultural equipment. As a result, farmers often use leftover crop residue as livestock feed or, less advisably, resort to burning them. Utilizing residue as feed presents no adverse effects and proves especially useful during winter months when other feed sources may be scarce. However, burning residue inflicts considerable damage on both the environment and public health. Therefore, reallocating residue scheduled for burning from one field to another for different purposes emerges as a viable alternative strategy.

It is crucial to recognize that the successful adoption of CA practice necessitates the application of all three foundational principles. The act of transporting residue complicates the assessment of whether no-till practices are applied prior to the crop being planted. As demonstrated by our experiment, it is feasible to move residue to fields regardless of whether they have been tilled. Transferring residue to fields that have not undergone tillage may enhance CA practice, whereas its application to tilled fields can confer benefits for TA practice. Consequently, we suggested

defining the concept of Transferred Crop Residue Cover (TCRC) and advocated for its inclusion as an auxiliary principle applicable to both CA and TA practices. While the comprehensive agronomic and environmental impacts of the approach require further investigation, we are optimistic about its broad-scale positive potential.

Limitations

The primary limitation of the study is the small field sampling area, which may not adequately represent the broader geographic diversity or capture the full variability in CRC areas. The constraint limits the generalizability of the findings and may affect the accuracy and applicability of the results to other regions or larger scales. Nonetheless, it should be noted that high spatial resolution data was utilized, offering precise local insights and detailed observations that are crucial for understanding specific site characteristics and small-scale variability (White & Roy, 2015). The use of high-resolution imagery partially compensates for the small sampling area by enhancing the accuracy of the data within the studied location.

The second limitation of the research might be the use of the blue band in the newly developed index. The PlanetScope constellation may not consistently provide the blue band reflectance time series (Huang & Roy, 2021) required for the current analyses due to its notable sensitivity to atmospheric scattering (Fraser & Kaufman, 1985), even after the atmospheric correction process. The susceptibility can introduce noise to the index, particularly under conditions with high atmospheric aerosols, potentially affecting the accuracy of crop residue detection. To address the limitation and improve the index's robustness, future enhancements might consider strategies employed by other vegetation indices that have successfully mitigated similar challenges. A prime example is the Enhanced Vegetation Index (EVI) (Huete et al., 1999), which incorporates the blue band specifically for aerosol correction in the red channel. EVI uses coefficients C_1 and C_2 to modulate the blue band's contribution, effectively reducing the impact of atmospheric conditions on vegetation signal retrieval. Inspired by EVI's approach, future iterations of NDCRI could explore incorporating an aerosol correction mechanism that leverages the blue band to adjust for atmospheric distortions.

The third potential limitation in our study may relate to moisture content. Soil and crop residue moisture levels can influence reflectance spectra, as noted by Hively et al. (2018). Regrettably, we lack moisture data to evaluate its influence on our index. However, given that field measurements were conducted during a period (August 10, 2022) without rainfall (Figure 9) and the new index

was developed considering the context, its temporal analysis (also during rainy periods) demonstrated that the effect of moisture content on the index's performance was not significantly in the maps produced.

Future Prospects

Undoubtedly, the future of CA and particularly the monitoring of CRC is linked with artificial intelligence (AI). The integration of AI techniques can significantly enhance the precision and efficiency of identifying and quantifying CRC across diverse landscapes. By leveraging machine learning algorithms and deep learning models, it is possible to analyze satellite imagery and other remote sensing data with unprecedented detail and accuracy.

The research by Sudheer et al. (2010), Ding et al. (2020), Najafi et al. (2021), Tao et al. (2021), Kazemi Garajeh et al. (2023), and Wang et al. (2023) has demonstrated productive employment of AI in assessing CRC. However, instances of AI-driven CRC detection primarily leveraging only visible and NIR bands remain scarce. Given its high spatial resolution, the PlanetScope constellation with bands from coastal blue to NIR emerges as an almost ideal platform for the task. By integrating AI methodologies with the spectral data from PlanetScope, researchers can unlock sophisticated models that can discern subtle differences in residue cover, even in challenging conditions. The potential for AI to automate the analysis process not only speeds up the monitoring tasks but also reduces the likelihood of human error, ensuring that conservation agriculture benefits from precise, data-driven decisions.

CHAPTER 5: CONCLUSION

Conservation Agriculture (CA) promotes a comprehensive farming approach that emphasizes the health of the soil and the wider ecosystem, securing long-term agricultural sustainability. By maintaining crop residues on fields, CA enhances various ecological functions such as improving soil structure, minimizing erosion, and encouraging biodiversity. Precisely measuring crop residue cover (CRC) is crucial for enacting effective soil conservation strategies, optimizing water utilization, and increasing organic matter.

However, numerous remote sensing technologies, including airbornes and satellites, face challenges in delivering detailed and timely data on CRC owing to limitations in spatial coverage and both temporal and spatial resolution. Considering the demands, the study employed the PlanetScope constellation, known for its daily availability of 3-meter resolution observations, for the first time to monitor CRC in the study area situated within the Urtachirchik District of Tashkent Province, Uzbekistan. Due to the PlanetScope sensors lacking the shortwave infrared (SWIR) bands necessary for detecting CRC and almost all previously developed formulas being associated with SWIR band, 16 spectral indices were formulated as candidates for a new crop residue index, named as the Normalized Difference Crop Residue Index (NDCRI), by utilizing four bands (yellow, red, red-edge, NIR) known for their high spectral reflectance in CRC sites and substantial differentiation between areas with and without CRC on one side, four bands (coastal blue, blue, green_i, green) that show low spectral reflectance in CRC locations and minimal differentiation between areas with and without CRC on the other side. Subsequently, the indices created as normalized ratios between two bands were individually compared to field measurements (n=20) for the purpose of identifying the band combination with the optimal correlation. As a result, the band duo (Red-Blue)/(Red+Blue), exhibiting the highest coefficient of determination (R^2=0.6934) and the lowest root mean squared error (RMSE=19.15) across all evaluated spectral indices in the polynomial fit of the second order, was confirmed as the basis for the newly formulated crop residue index (NDCRI). The absence of uniform trends in the residuals, coupled with the closely normal distribution observed mainly within the mid-section of the Q-Q plot, indicated that the NDCRI effectively captures the variance in the crop residue fraction.

Further, NDCRI was applied to images of both the study area and the entire Urtachirchik District on various days for mapping residue cover. For the classification of residue cover, it was important to mask all areas displaying an Normalized Difference Vegetation Index (NDVI) value greater

than 0.22 (determined by comparing the green-up, mature, and residue periods of winter wheat in the study) to reduce the impact of vegetation on the detection of crop residue.

Moreover, we suggested the concept of Transferred Crop Residue Cover (TCRC) and advocated for its inclusion as an auxiliary principle applicable to both conservation and traditional agriculture practices.

Despite the limitations associated with using the blue band in the new index (due to atmospheric scattering) and the absence of moisture content data, the research highlighted the robust capabilities of PlanetScope satellite imagery for CA. By introducing NDCRI, the study not only addressed the crucial aspect of crop residue monitoring but also set a new benchmark for remote sensing applications in agriculture. Conclusively, the work laid a solid foundation for future advancements, strongly indicating that the integration of artificial intelligence (AI) with remote sensing data stands as the next frontier in the efficient and sophisticated monitoring of CRC, heralding a new era of precision in conservation agriculture.

BIBLIOGRAPHY

Abatzoglou, J. T., Dobrowski, S. Z., Parks, S. A., & Hegewisch, K. C. (2018). TerraClimate, a high-resolution global dataset of monthly climate and climatic water balance from 1958–2015. *Scientific data*, *5*(1), 1-12.

Asner, G. P., & Lobell, D. B. (2000). A biogeophysical approach for automated SWIR unmixing of soils and vegetation. *Remote sensing of environment*, *74*(1), 99-112.

Azzari, G., Grassini, P., Edreira, J. I. R., Conley, S., Mourtzinis, S., & Lobell, D. B. (2019). Satellite mapping of tillage practices in the North Central US region from 2005 to 2016. *Remote Sensing of Environment*, *221*, 417-429.

Bannari, A., Pacheco, A., Staenz, K., McNairn, H., & Omari, K. (2006). Estimating and mapping crop residues cover on agricultural lands using hyperspectral and IKONOS data. *Remote sensing of environment*, *104*(4), 447-459.

Ben-Dor, E., Heller, D., & Chudnovsky, A. (2008). A novel method of classifying soil profiles in the field using optical means. *Soil Science Society of America Journal*, *72*(4), 1113-1123.

Blinn, M., Lautenbach, S., Grade, J., Lennartz, G., Fischer, A., Weiss, D., & Kötter, T. (2022). How to Grow? -Modeling Land Use Change to Develop Sustainable Pathways for Settlement Growth in the Hinterland of Cologne, Germany. *The International Archives of the Photogrammetry, Remote Sensing and Spatial Information Sciences*, *48*, 67-72.

Bonham, C. D. (1989). *Measurements for terrestrial vegetation*. John Wiley & Sons.

Cao, X., Chen, J., Matsushita, B., & Imura, H. (2010). Developing a MODIS-based index to discriminate dead fuel from photosynthetic vegetation and soil background in the Asian steppe area. *International Journal of Remote Sensing*, *31*(6), 1589-1604.

Claverie, M., Ju, J., Masek, J. G., Dungan, J. L., Vermote, E. F., Roger, J. C., ... & Justice, C. (2018). The Harmonized Landsat and Sentinel-2 surface reflectance data set. *Remote sensing of environment*, *219*, 145-161.

CTIC. (2022). *Tillage Type Definitions*. Retrieved March 16, 2024, from https://www.ctic.org/resource_display/?id=322&title=Tillage+Type+Definitions.

Daughtry, C. S. (2001). Discriminating crop residues from soil by shortwave infrared reflectance. *Agronomy Journal*, *93*(1), 125-131.

Daughtry, C. S. T., Hunt Jr, E. R., & McMurtrey Iii, J. E. (2004). Assessing crop residue cover using shortwave infrared reflectance. *Remote Sensing of Environment*, *90*(1), 126-134.

Daughtry, C. S., Hunt Jr, E. R., Doraiswamy III, P. C., & McMurtrey, J. E. (2005). Remote sensing the spatial distribution of crop residues. *Agronomy Journal*, *97*(3), 864-871.

Daughtry, C. S., Doraiswamy, P. C., Hunt Jr, E. R., Stern, A. J., McMurtrey Iii, J. E., & Prueger, J. H. (2006). Remote sensing of crop residue cover and soil tillage intensity. *Soil and Tillage Research*, *91*(1-2), 101-108.

Delgado, J. A. (2010). Crop residue is a key for sustaining maximum food production and for conservation of our biosphere. *journal of soil and water conservation*, *65*(5), 111A-116A.

Devkota, M., Martius, C., Lamers, J. P. A., Sayre, K. D., Devkota, K. P., Gupta, R. K., ... & Vlek, P. L. (2013). Combining permanent beds and residue retention with nitrogen fertilization improves crop yields and water productivity in irrigated arid lands under cotton, wheat and maize. *Field Crops Research*, *149*, 105-114.

Devkota, M., Gupta, R. K., Martius, C., Lamers, J. P. A., Devkota, K. P., Sayre, K. D., & Vlek, P. L. G. (2015). Soil salinity management on raised beds with different furrow irrigation modes in salt-affected lands. *Agricultural Water Management*, *152*, 243-250.

Ding, Y., Zhang, H., Wang, Z., Xie, Q., Wang, Y., Liu, L., & Hall, C. C. (2020). A comparison of estimating crop residue cover from sentinel-2 data using empirical regressions and machine learning methods. *Remote Sensing*, *12*(9), 1470.

Egamberdiev, O. (2007). *Changes of soil characteristics under the influence of resource-saving and soil-protective technologies within irrigated meadow alluvial soil of the Khorezm region*. State Research Institute of Soil Science and Agrochemistry Tashkent, Uzbekistan, Ph.D. dissertation, pp. 200.

ESRI. (2022). *ArcGIS Desktop 10.8.2*. Redlands, CA, USA.

ESRI. (2022). *ArcGIS Pro Release 3.0.0*. Redlands, CA, USA.

Fabre, S., Briottet, X., & Lesaignoux, A. (2015). Estimation of soil moisture content from the spectral reflectance of bare soils in the 0.4–2.5 µm domain. *Sensors*, *15*(2), 3262-3281.

FAO. (2009). *Conservation agriculture in Uzbekistan*. Food and Agriculture Organization of the United Nations, Rome, pp. 23–25, pp. 29–30.

FAO. (2011). *The state of the world's land and water resources for food and agriculture (SOLAW) - Managing systems at risk*. Food and Agriculture Organization of the United Nations, Rome and Earthscan, London.

FAO. (2023). *Uzbekistan: Roadmap to Tackle Climate Change Challenges to Agricultural Production*. Retrieved March 15, 2024, from https://www.fao.org/science-technology-and-innovation/resources/stories/detail/uzbekistan--roadmap-to-tackle-climate-change-challenges-to-agricultural-production.

FAO. (2024). *Conservation Agriculture*. Retrieved March 15, 2024, from https://www.fao.org/conservation-agriculture/en.

Fraser, R. S., & Kaufman, Y. J. (1985). The relative importance of aerosol scattering and absorption in remote sensing. *IEEE transactions on geoscience and remote sensing*, (5), 625-633.

Gao, L., Zhang, C., Yun, W., Ji, W., Ma, J., Wang, H., ... & Zhu, D. (2022). Mapping crop residue cover using Adjust Normalized Difference Residue Index based on Sentinel-2 MSI data. *Soil and Tillage Research*, *220*, 105374.

Gausman, H. W., Gerbermann, A. H., Wiegand, C. L., Leamer, R. W., Rodriguez, R. R., & Noriega, J. R. (1975). Reflectance differences between crop residues and bare soils. *Soil Science Society of America Journal*, *39*(4), 752-755.

Gelder, B. K., Kaleita, A. L., & Cruse, R. M. (2009). Estimating mean field residue cover on midwestern soils using satellite imagery. *Agronomy journal*, *101*(3), 635-643.

Gerts, J., Juliev, M., & Pulatov, A. (2020). Multi-temporal monitoring of cotton growth through the vegetation profile classification for Tashkent province, Uzbekistan. *GeoScape*, *14*(1), 62-69.

Godwin, R. J. (1990). *Agricultural engineering in development: tillage for crop production in areas of low rainfall* (No. 83, pp. 124-pp).

Gowda, P. H., Dalzell, B. J., Mulla, D. J., & Kollman, F. (2001). Mapping tillage practices with landstat thematic mapper based logistic regression models. *Journal of Soil and Water Conservation*, *56*(2), 91-96.

Hively, W. D., Lamb, B. T., Daughtry, C. S., Shermeyer, J., McCarty, G. W., & Quemada, M. (2018). Mapping crop residue and tillage intensity using WorldView-3 satellite shortwave infrared residue indices. *Remote Sensing*, *10*(10), 1657.

Hobbs, P. R., Sayre, K., & Gupta, R. (2008). The role of conservation agriculture in sustainable agriculture. *Philosophical Transactions of the Royal Society B: Biological Sciences*, *363*(1491), 543-555.

Hoekstra, A. Y., & Wiedmann, T. O. (2014). Humanity's unsustainable environmental footprint. *Science*, *344*(6188), 1114-1117.

Huang, H., & Roy, D. P. (2021). Characterization of Planetscope-0 Planetscope-1 surface reflectance and normalized difference vegetation index continuity. *Science of remote sensing*, *3*, 100014.

Huete, A., Justice, C., & Van Leeuwen, W. (1999). MODIS vegetation index (MOD13). *Algorithm theoretical basis document*, *3*(213), 295-309.

IPCC. (2022). Climate Change 2022: Impacts, Adaptation, and Vulnerability. Contribution of Working Group II to the Sixth Assessment Report of the Intergovernmental Panel on Climate Change [Pörtner, H. O., Roberts, D. C., Tignor, M., Poloczanska, E. S., Mintenbeck, K., Alegría, A., Craig, M., Langsdorf, S., Löschke, S., Möller, V., Okem, A., Rama, B. (eds.)]. *Cambridge University Press*. Cambridge University Press, Cambridge, UK and New York, NY, USA, 3056 pp., doi:10.1017/9781009325844.

Kazemi Garajeh, M., Hassangholizadeh, K., Bakhshi Lomer, A. R., Ranjbari, A., Ebadi, L., & Sadeghnejad, M. (2023). Monitoring the impacts of crop residue cover on agricultural productivity and soil chemical and physical characteristics. *Scientific Reports*, *13*(1), 15054.

Khaitov, B., & Allanov, K. (2014). Crop rotation with no-till methods in cotton production of Uzbekistan. *Eurasian journal of soil Science*, *3*(1), 28-32.

Kosmowski, F., Stevenson, J., Campbell, J., Ambel, A., & Haile Tsegay, A. (2017). On the ground or in the air? A methodological experiment on crop residue cover measurement in Ethiopia. *Environmental management*, *60*, 705-716.

LexUZ. (2019). *PD-5853. The Strategy for the Development of Agriculture in the Republic of Uzbekistan for 2020-2030*. Retrieved March 17, 2024, from https://lex.uz/docs/-4567334.

McNairn, H., & Protz, R. (1993). Mapping corn residue cover on agricultural fields in Oxford County, Ontario, using Thematic Mapper. *Canadian Journal of Remote Sensing*, *19*(2), 152-159.

Mirshadiev, M. (2015). *Land and Water use change assessment in Tashkent province, Uzbekistan*. Wageningen University, Netherlands, Master Thesis report MIL-2015-00, pp. 61.

Morrison, J. E., Huang, C. H., Lightle, D. T., & Daughtry, C. S. (1993). Residue measurement techniques. *Journal of soil and water conservation*, *48*(6), 478-483.

Nagler, P. L., Inoue, Y., Glenn, E. P., Russ, A. L., & Daughtry, C. S. T. (2003). Cellulose absorption index (CAI) to quantify mixed soil–plant litter scenes. *Remote Sensing of Environment*, *87*(2-3), 310-325.

Najafi, P., Feizizadeh, B., & Navid, H. (2021). A comparative approach of fuzzy object based image analysis and machine learning techniques which are applied to crop residue cover mapping by using Sentinel-2 satellite and UAV imagery. *Remote Sensing*, *13*(5), 937.

Papendick, R. I., Parr, J. F., & Meyer, R. E. (1990). Managing crop residues to optimize crop/livestock production systems for dryland agriculture. *Advances in Soil Science: Dryland Agriculture: Strategies for Sustainability Volume 13*, 253-272.

Pender, J., Mirzabaev, A., & Kato, E. (2009). Economic analysis of sustainable land management options in Central Asia. *Final report for the ADB. IFPRI/ICARDA*, *168*.

Pepe, M., Pompilio, L., Gioli, B., Busetto, L., & Boschetti, M. (2020). Detection and classification of non-photosynthetic vegetation from PRISMA hyperspectral data in croplands. *Remote Sensing*, *12*(23), 3903.

Philpot, W. (2014, July). Spectral reflectance of drying, sandy soils. In *2014 IEEE Geoscience and Remote Sensing Symposium* (pp. 3642-3645). IEEE.

Pilger, N., Berg, A., & Joosse, P. (2020). Semi-automated roadside image data collection for characterization of agricultural land management practices. *Remote Sensing*, *12*(14), 2342.

Planet Developers. (2024). *Understanding PlanetScope Instruments*. Retrieved March 18, 2024, from https://developers.planet.com/docs/apis/data/sensors.

Planet Team. (2023). *PlanetScope Product Specifications*. Retrieved March 18, 2024, from https://assets.planet.com/docs/Planet_PSScene_Imagery_Product_Spec_letter_screen.pdf.

Pulatov, A. (2007). Enhanced productivity of cotton-wheat systems through adoption of conservation agriculture practices. *FAO/TCP/UZB/001 Project Final Report*. Tashkent, Uzbekistan: Tashkent Institute of Irrigation and Melioration.

Pulatov, A., Egamberdiev, O., Karimov, A., Tursunov, M., Kienzler, S., Sayre, K., ... & Martius, C. (2012). Introducing conservation agriculture on irrigated meadow alluvial soils (Arenosols) in Khorezm, Uzbekistan. *Cotton, water, salts and Soums: economic and ecological restructuring in Khorezm, Uzbekistan*, 195-217.

Pulatov A.S. et al. (in press). Energy – Water – Fertilizer – Ecosystem Saving Intelligent - Automated Systems for Irrigated Conservation Agriculture Areas in Uzbekistan. *Research report*. MHESI grant A-OT-2021-32, pp. 147.

Ranaivoson, L., Naudin, K., Ripoche, A., Affholder, F., Rabeharisoa, L., & Corbeels, M. (2017). Agro-ecological functions of crop residues under conservation agriculture. A review. *Agronomy for sustainable development*, *37*, 1-17.

Rouse, J. W., Haas, R. H., Schell, J. A., & Deering, D. W. (1974). Monitoring vegetation systems in the Great Plains with ERTS. *NASA Spec. Publ*, *351*(1), 309.

Serbin, G., Hunt Jr, E. R., Daughtry, C. S., McCarty, G. W., & Doraiswamy, P. C. (2009a). An improved ASTER index for remote sensing of crop residue. *Remote Sensing*, *1*(4), 971-991.

Serbin, G., Daughtry, C. S., Hunt Jr, E. R., Reeves III, J. B., & Brown, D. J. (2009b). Effects of soil composition and mineralogy on remote sensing of crop residue cover. *Remote Sensing of Environment*, *113*(1), 224-238.

Sims, J. T., Ma, L., Oenema, O., Dou, Z., & Zhang, F. S. (2013). Advances and challenges for nutrient management in China in the 21st century. *Journal of environmental quality*, *42*(4), 947-950.

Somasundaram, J., Sinha, N. K., Dalal, R. C., Lal, R., Mohanty, M., Naorem, A. K., ... & Chaudhari, S. K. (2020). No-till farming and conservation agriculture in South Asia–issues, challenges, prospects and benefits. *Critical Reviews in Plant Sciences*, *39*(3), 236-279.

Sudheer, K. P., Gowda, P., Chaubey, I., & Howell, T. (2010). Artificial neural network approach for mapping contrasting tillage practices. *Remote Sensing*, *2*(2), 579-590.

Sullivan, D. G., Truman, C. C., Schomberg, H. H., Endale, D. M., & Strickland, T. C. (2006). Evaluating techniques for determining tillage regime in the Southeastern Coastal Plain and Piedmont. *Agronomy journal*, *98*(5), 1236-1246.

Tao, W., Xie, Z., Zhang, Y., Li, J., Xuan, F., Huang, J., ... & Yin, D. (2021). Corn Residue Covered Area Mapping with a Deep Learning Method Using Chinese GF-1 B/D High Resolution Remote Sensing Images. *Remote Sensing*, *13*(15), 2903.

The World Bank. (2024). *Agriculture and Food. Overview*. Retrieved March 15, 2024, from https://www.worldbank.org/en/topic/agriculture/overview.

Thoma, D. P., Gupta, S. C., & Bauer, M. E. (2004). Evaluation of optical remote sensing models for crop residue cover assessment. *Journal of soil and water conservation*, *59*(5), 224-233.

UN. (2015). *Transforming Our World: The 2030 Agenda for Sustainable Development*. Retrieved March 15, 2024, from https://sdgs.un.org/2030agenda.

USDA. (2024). *Crop Calendar Charts*. Retrieved March 15, 2024, from https://ipad.fas.usda.gov/ogamaps/cropcalendar.aspx.

UZSTAT. (2023). *The Production of Crop and Livestock Products in All Categories of Farms in the Republic of Uzbekistan*. Retrieved March 15, 2024, from https://stat.uz/uz/rasmiy-statistika/agriculture-2.

Van Deventer, A. P., Ward, A. D., Gowda, P. H., & Lyon, J. G. (1997). Using thematic mapper data to identify contrasting soil plains and tillage practices. *Photogrammetric engineering and remote sensing*, *63*, 87-93.

Van Dijk, M., Morley, T., Rau, M. L., & Saghai, Y. (2021). A meta-analysis of projected global food demand and population at risk of hunger for the period 2010–2050. *Nature Food*, *2*(7), 494-501.

Van Rossum, G., & Drake, F. L. (2009). *Python 3 Reference Manual*. Scotts Valley, CA: CreateSpace.

Verrelst, J., Halabuk, A., Atzberger, C., Hank, T., Steinhauser, S., & Berger, K. (2023). A comprehensive survey on quantifying non-photosynthetic vegetation cover and biomass from imaging spectroscopy. *Ecological Indicators*, *155*, 110911.

Wang, S., Guan, K., Zhang, C., Zhou, Q., Wang, S., Wu, X., ... & Ma, Z. (2023). Cross-scale sensing of field-level crop residue cover: Integrating field photos, airborne hyperspectral imaging, and satellite data. *Remote Sensing of Environment*, *285*, 113366.

Watts, J. D., Powell, S. L., Lawrence, R. L., & Hilker, T. (2011). Improved classification of conservation tillage adoption using high temporal and synthetic satellite imagery. *Remote Sensing of Environment*, *115*(1), 66-75.

White, E. V., & Roy, D. P. (2015). A contemporary decennial examination of changing agricultural field sizes using Landsat time series data. *Geo: Geography and environment*, *2*(1), 33-54.

Wocher, M., Berger, K., Danner, M., Mauser, W., & Hank, T. (2018). Physically-based retrieval of canopy equivalent water thickness using hyperspectral data. *Remote Sensing*, *10*(12), 1924.

Yue, J., Tian, Q., Dong, X., Xu, K., & Zhou, C. (2019). Using hyperspectral crop residue angle index to estimate maize and winter-wheat residue cover: A laboratory study. *Remote Sensing*, *11*(7), 807.

Yue, J., Tian, Q., Dong, X., & Xu, N. (2020). Using broadband crop residue angle index to estimate the fractional cover of vegetation, crop residue, and bare soil in cropland systems. *Remote sensing of environment*, *237*, 111538.

Zheng, B., Campbell, J. B., & de Beurs, K. M. (2012). Remote sensing of crop residue cover using multi-temporal Landsat imagery. *Remote Sensing of Environment*, *117*, 177-183.

Zheng, B., Campbell, J. B., Serbin, G., & Galbraith, J. M. (2014). Remote sensing of crop residue and tillage practices: Present capabilities and future prospects. *Soil and Tillage Research*, *138*, 26-34.

Zhou, W., Rao, P., Jat, M. L., Singh, B., Poonia, S., Bijarniya, D., ... & Jain, M. (2021). Using Sentinel-2 to track field-level tillage practices at regional scales in smallholder systems. *Remote Sensing*, *13*(24), 5108.